Reflectance Studies of Ba, Sr, Eu, and Yb†‡

J. G. Endriz and W. E. Spicer
Stanford Electronics Laboratories, Stanford University, Stanford, California 94305
(Received 30 January 1970)

In situ reflectance measurements have been made on films of the alkaline-earth metals barium (bcc) and strontium (fcc), and rare-earth metals europium (bcc) and ytterbium (fcc) from 1.0 to 11.6 eV. Extreme care was taken in all aspects of the work so that a Kramers-Krönig analysis of the reflectance data yielded optical constants ϵ_1, ϵ_2, σ, and α which were accurate to better than ± 20%. The volume-loss functions calculated from these optical constants yielded an agreement with loss-function peak positions obtained in Kunz's high-energy electron-loss experiments which was not seen in previous optical studies, and served as verification of the improved accuracy of the present study. A comparison of the interband optical conductivities for the alkaline-earth and rare-earth metals failed to indicate strong structure or increased oscillator strength in the rare-earth metals which could be unambiguously attributed to transitions from 4*f* electrons found in europium and ytterbium. The filled 4*f*-electron states in these two metals are known to be accessible to the spectral range of the present study, and an explanation, based on matrix elements, is proposed for this inability to excite such electrons. The structure which was observed in the interband conductivity of all four of these metals was correlated to crystal structure and showed much better agreement with the predictions of strong *d*-electron effects implied in recent band calculations than it did with the simple predictions of the nearly-free-electron theory.

I. INTRODUCTION

Comparative studies of the alkaline-earth metals, barium (Ba), and strontium (Sr), and the divalent rare-earth metals, europium (Eu) and ytterbium (Yb), have become of increasing interest over the last few years owing to the strong similarities in electronic structure of these four metals.

The lanthanons are normally trivalent, but the strong preference for a symmetric 4*f* shell in these metals results in a ground state for atomic Eu which is divalent with a half-filled 4*f*-electron shell, and a ground state for Yb which is divalent with a filled 4*f*-electron shell. Metallic Eu has a body-centered-cubic (bcc) crystal structure and should differ from divalent bcc Ba primarily in the presence of its half-filled 4*f*-electron shell. Metallic Yb has a face-centered-cubic (fcc) crystal structure and should differ from divalent fcc Sr primarily in the presence of its filled 4*f*-electron shell.[1] These effects, along with the atomic valence configurations of these metals, are shown in the periodic chart of Fig. 1.

The present study consists of optical-reflectance studies of all four of these metals over an energy range from 1.0 to 11.6 eV. A Kramers-Krönig analysis has been carried out on these measurements and the optical constants obtained over this same spectral region.

It was hoped that by comparing the results of these optical studies on Eu and Yb with the results obtained for Ba and Sr that those properties resulting from transitions from 4*f*-electron shells could be isolated. In the same vein, it was felt that by comparing the optical properties of the two fcc metals with those obtained for the bcc materials, that those effects dependent upon crystal structure could be determined.

Interest in the observation of transitions from the 4*f* electrons in the rare earths stems from the inability of theoretical calculations to accurately predict these 4*f*-energy levels.[2] While atomic-energy-level calculations[3] and recent band calculations[2] have all implied that the 4*f* electrons should lie close enough to the Fermi level in Eu and Yb to

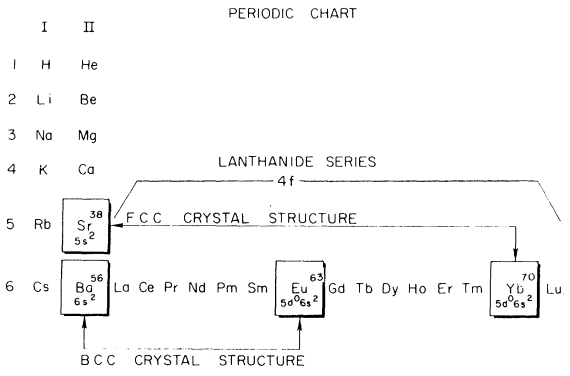

FIG. 1. Periodic chart showing the similarities in electronic and crystal structure of the four materials under study.

be observable in the present study, an exact prediction of these $4f$ energy levels has been hampered by the inability to accurately handle exchange effects in such tightly bound states.

The need for experimental information relating to the fcc and bcc crystal structures of these metals arises from the lack of an appreciable amount of experimental data which can presently be compared to recent band-structure calculations on Ba, Sr, and Eu. The highly reactive nature of all of these elements has prevented extensive studies in the past. The optical constants of Ba were first measured in rather low vacuum by Maurer. [4] Since then the measurements on Ba have been extended into the uv by Fisher *et al.*[5] What probably stands as the best prior study on these four metals was carried out by Müller. [6,7] Both transmission and reflectance were measured from 0.5 to 5.0 eV on all four metals, and the optical conductivities were derived over this same spectral range. Müller noted strong similarities between the two fcc metals and between the two bcc metals, and found qualitative agreement between the position of structure observed in Eu and the position of such structure as implied in the recent band calculation on Eu by Freeman *el al.* [8] An important characteristic of this band calculation on Eu, as well as those previously completed on Ba[9,10] and Sr, [10] is the presence of strong d-band mixing and s-d hybridization near or just above the Fermi level.

It was thus hoped that the results of the present study could be used to confirm the observations of Müller over the energy range below 5.0 eV, and to extend the search for transitions from the $4f$ states and for structure which might be attributed to strong d-band mixing out to the far uv. In actual fact, the reflectance values reported in the present paper were found to be of considerably higher value and in significant disagreement with all previous reflectance measurements on these four metals. Because of these strong differences and the fact that Müller's measurements were made with a highly accurate reflectometer incorporating compensating-mirror systems, [11] a careful analysis of the preparation techniques and errors associated with the uv reflectometer used in the present study was carried out. A detailed description of these and other important experimental problems associated with the present study appears in Sec. II. This discussion is considered a necessary prologue to the experimental results and physical interpretations reported in this paper.

II. EXPERIMENTAL TECHNIQUE AND REFLECTANCE

An appreciation of the results of the reflectance measurements reported in this paper can be gained only by noting the discrepancies between these results and the reflectance measurements performed on these same materials by earlier authors [5,6] (see Sec. II C). The present results should not and cannot be accepted without a careful examination and justification of the experimental technique used to achieve them. Foremost among these techniques is the method used to measure reflectance. Müller's measurements were made in the *sapphire* ultraviolet range, and thus he was able to use a reflectometer incorporating systems of compensating mirrors capable of yielding accuracies well within $\pm 1\%$ R. The present study was carried out to the far uv (11.6 eV) and suffered from all the hazards inherent in measuring reflectance in that spectral range. Despite these unique problems, a far uv reflectometer was designed capable of measuring reflectance accurate to $\pm 1\%$ R. An explanation of the problems involved in this design follows.

Of comparable importance in justifying the present results in light of the measurements by Müller is the problem of surface conditions of the materials studied. Vaccuum preparation and film-growth techniques were developed which can ensure smooth surfaces and a total surface contamination during sample preparation and measurement of less than one monolayer. Because of the highly reactive nature of all four of the materials studied and the unique problems which this poses, a discussion of the means by which our samples were prepared is also included.

A more detailed analysis of the uv reflectometer and preparation techniques is available, [12] and thus only the most important techniques are included in the present discussion.

A. Ultraviolet Reflectometer

1. *Basic Reflectometer Design*

The design of the uv reflectometer used in these measurements is shown diagrammatically in Fig. 2. The apparatus shown is enclosed in an ultra-high-vacuum system with a LiF window which allows transmission out to 11.6 eV. A McPherson model 225 1-m vacuum uv monochromator with a Hinteregger-type capillary discharge tube is used as a source from 2.2 to 11.6 eV, while a Bausch and Lomb 500-mm visible monochromator with tungsten-filament light source is used from 3.5 down to 1.0 eV.

The aperture shown serves to limit the light-spot size, and thus better define its position. This in turn reduces the effects of monochromator beam inhomogeneities. The sodium salicylate phosphor – light pipe – phototube system may then be used as a light detection system, where the phototube used responds to the fluorescence spectrum

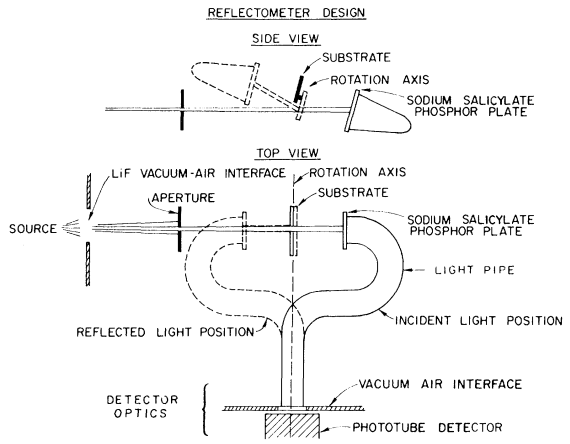

FIG. 2. Basic design of the uv reflectometer used in the present study.

of the phosphor for uv frequencies. At monochromator frequencies below the fluorescence onset of sodium salicylate (3.5-eV photon energy), the phototube must detect the monochromator frequency directly. Electronic detection of the phototube current is accomplished using a modified counting system which allows an effective integration time of 10, 20, or 30 sec.

Incident- and reflected-light intensities are detected with the light pipe in the positions shown in the figure. Rotation of the light pipe and substrate between these two positions is accomplished via a magnetic coupling through thin stainless-steel walls which preserve the ultrahigh vacuum. The position of the substrate is adjustable in all dimensions so that the light beam may be made to strike the light-pipe face at the same position, and made to enter at the same angle in both incident and reflect positions. Because the substrate lies on the light-pipe rotational axis, the divergence of the light beam, and thus the spot size on the light-pipe face, is also the same in both incident and reflect positions. The reflectometer, thus, provides a method which, in theory, allows the measurement of the ratio of incident- and reflected-light intensities independent of source or detector response variations. In actual fact, this type of reflectometer detection system has many peculiarities not found in more sophisticated reflectometers having frequencies of operation which allow the use of compensating-lens and mirror systems. Errors in reflectivity on the order of $\pm 5\%$ were found to exist in the above system prior to a careful analysis and correction of the major problems.

2. *Estimation of Error*

The dominant sources of error in the operation of the reflectometer may be conveniently divided into (i) errors arising from the detector optics (see Fig. 2), (ii) errors associated with the monochromator–light-pipe optics up to the detection system, and (iii) errors resulting from anomalies in the properties of the sodium salicylate phosphor.

The most serious of these three error sources is the monochromator–light-pipe optics. Most optics and light-beam problems effect the accuracy of the reflectometer only to the extent that the light-pipe transmission is sensitive to the position at which the light beam strikes its face. For this reason, light-pipe beam-position response was found to be of critical importance in limiting predetector-optics errors. We have found that by using a light pipe having three distinct right-angle bends, as seen in Fig. 2, we can obtain a pipe whose transmission varies by less than 10% as one scans the center third of the pipe face. Light-beam-position uncertainties, alignment limitations, and monochromator-beam inhomogeneities couple to this residual light-pipe transmission sensitivity to yield an error in the predetector optics measured at $< \pm 1.05\%$.

Of lesser importance to the accurate operation of the reflectometer were errors associated with the detector optics. Lack of cylindrical symmetry in the detector optics (arising primarily from photocathode inhomogeneities) introduced significant errors as the light pipe was rotated from the incident position to the reflect position. These errors were reduced to $< \pm 0.35\%$ by designing a phototube mount which could be rotated coaxially with the light tube.

Very serious errors were found to arise from heat deterioration of the sodium salicylate, and from an apparent severe decrease in the response of the phosphor in the 3.4- to 3.6-eV spectral range. Deterioration problems were eliminated by using a laminated Cu-Al heat shield during evaporations and by keeping bake-out temperatures below 180 °C. The response drop between 3.4 and 3.6 eV apparently arose from absorption of light without the luminescence which occurs above 3.6 eV. The solution was to avoid problems, such as scattered light, which are of general concern in low-sensitivity regions.

Residual errors associated with sodium salicylate anomalies are too small to measure, while residual errors associated with the reflectometer-detector optics, predetector optics, and electronic noise yield a total expected reflectance uncertainty in reflectometer measurements of $< \pm 1.2\%$.

Verification of these estimates is given in the reflectance results shown in Fig. 3. The amorphous germanium (Ge) and aluminum (Al) film reflectivities have been recently measured on the

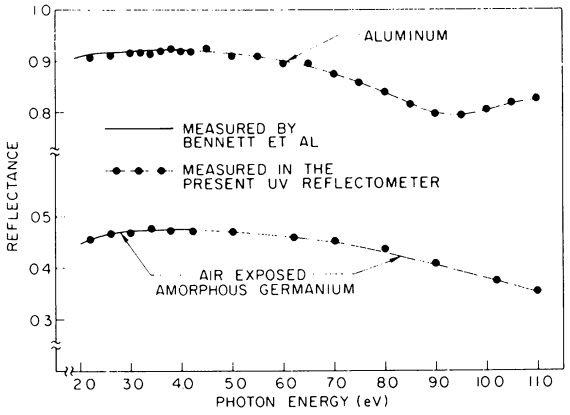

FIG. 3. Comparison of reflectance values for aluminum and amorphous germanium measured on the reflectometer used in the present study with the reflectance values obtained for these two materials by H. E. Bennett *et al.* (private communication) on their highly accurate (±0.1%) visible reflectometer.

uv reflectometer under discussion. They are compared with measurements made on the highly accurate (± 0.1%) visible reflectometer at the Michelson Laboratory, China Lake, Calif. The amorphous Ge measurements were made on the same air-exposed sample by both reflectometers. The Al measurements were made on two different films prepared in a similar fashion. One notes that the reflectance values do, indeed, agree to within ± 1.0%.

B. Sample Preparation

Sample preparation is essentially concerned with providing a plane-surface pure sample having the physical properties of the bulk material – a sample which can be measured *in situ* with the reflectometer described above. The high reactivity of the metals under study makes thin-film evaporation virtually the only means of preparing such samples. That the resulting evaporated thin films do indeed have the properties of bulk crystalline samples has been verified in thin-film resistivity measurements by Schüller.[13]

1. *Pressure Contamination*

We see in Fig. 4 typical mass-spectrometer curves of (a) the gas constituents of the base pressure (5×10^{-11} Torr) of the NRC model 206 Orbion pumped stainless-steel chamber which houses the reflectometer and (b) the evaporation outgas spectrum (2×10^{-6} Torr) of one of the metals being studied. Most probable sources of mass peaks are given in parentheses.

The four metals studied were found to evaporate near their melting temperatures, and these temperatures were quite low in all cases (≤900 °C). For this reason it is felt that the large observed outgassing of H_2, CH_4, and N_2 during evaporation can be explained only in terms of decomposition of hydrides, carbides, and nitrides of the evaporants themselves. This severe outgassing was found to be intolerable from the standpoint of both bulk and surface contamination. The problem was solved by limiting the amount of evaporant heated. Small amounts of the metals were precondensed onto molybdenum cups which could then be transferred in argon to the reflectometer. The cups were

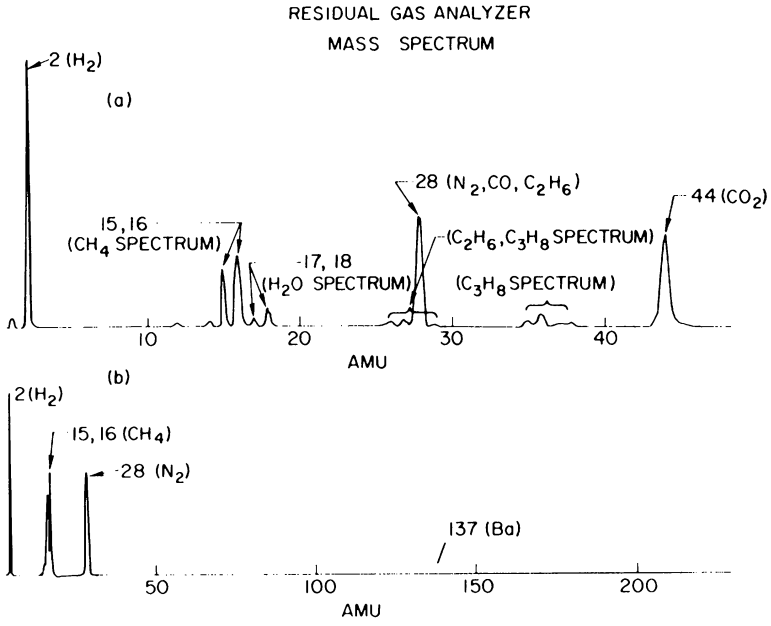

FIG. 4. Mass-spectrometer curves indicating [(a) – top curve] the gas constituents at the reflectometer base pressure ($\sim 5 \times 10^{-11}$ Torr) and [(b) – bottom curve] the gas constituents observed during an evaporation of one of the metals under study (Ba) at an evaporation pressure of 2×10^{-6} Torr. Probable origins of various peaks are given in parentheses.

TABLE I. Relevant parameters in the preparation of pure opaque films of the materials under study. Substantial evaporation from the metals was first noted just below their melting temperatures. Evaporations were carried out at ~ 1000 Å/min and base pressures of $< 5 \times 10^{-12}$ Torr were achieved within 1 min of the completion of the evaporation.

	Opacity thickness (Å)	Melting temperature (°C)	Evaporation pressure (Torr)
Ba	~2200	725	4×10^{-8}
Sr	~2000	769	2×10^{-8}
Eu	~1600	900	3×10^{-8}
Yb	~1300	825	1.2×10^{-8}

heated close enough to the substrate (1.7 in.) so that opaque films[14] could still be obtained. Pumping was augmented by liquid-N_2 cooling of the Orbion pump.

These procedures allowed deposition of each of the four metals at rates greater than 2000 Å/min and pressures $\leq 4 \times 10^{-8}$ Torr. Base pressures were on the 10^{-12}-Torr scale. These and other relevant preparation data are summarized in Table I. Bulk and surface gas contamination was calculated from the measured base and evaporation pressures, the measured gas constituents of Fig. 4, and the assumption of unit-sticking coefficient. The results of these calculations imply that none of the four metals could have accumulated more than a fraction of a surface-contaminant monolayer between the completion of the evaporation and the completion of the measurement. Mean distances between bulk impurity atoms were found to be significantly greater than estimates of the phonon scattering lengths for these materials. These results would seem to imply that our reflectance measurements cannot be significantly effected by either bulk or surface contamination in any of the metals studied.

Verification of this analysis of bulk and surface contamination is given with the curves of Ba reflectivity versus pressure shown on Fig. 5. Barium, which was the most seriously contaminated of the four metals, shows no appreciable change in reflectivity as the evaporation pressure is dropped from 8×10^{-8} to 4×10^{-8} Torr.

2. *Film Growth and Surface Roughness*

The possible adverse effects of surface roughness have been discussed in the literature with regard to diffuse scattering of reflected light, [15] and more recently with regard to possible roughness-aided coupling to surface losses. [16,17]

An application of the established theory of light scattering by roughened surfaces shows, for example, that 1.5% of an 11.6-eV reflected light beam would be diffusely scattered by a rough surface characterized by an root mean square (rms) height variation of only 10 Å. This effect drops off rapidly at lower frequencies, but drops in reflectance of considerably greater than 1% may occur as a result of roughness-aided optical coupling to surface plasmons at frequencies in the vicinity of the surface-plasma frequency. The Al reflectance of Fig. 3, for example, shows a quite large dip in reflectance from 7 to 11 eV which has been attributed to coupling to such surface losses. [18,19] These losses peak near 10 eV in Al. The rms height variation of the substrate which allowed this coupling was later measured by Bennett of the Michelson Laboratory, China Lake, Calif., and found to be approximately 12-15 Å.

It thus becomes obvious that rms height variation of the substrates used in our studies should be kept at less than 10 Å. An inexpensive method of obtaining very smooth substrates was suggested by Bennett. A new method of industrial glass production which involves floating the glass on molten tin yields glass surfaces which are extremely smooth on the surface in contact with the tin. Such "float glass" was obtained from Chance Pilkington Float Glass in Toronto, Canada. Substrates were machined from the glass, and the substrate surface measured for roughness at the Michelson Laboratory. The results of these measurements yielded

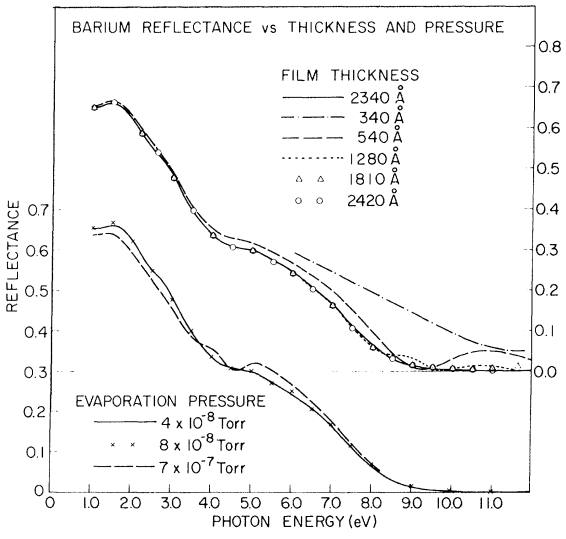

FIG. 5. Barium reflectance curves versus thickness and evaporation pressure indicate that reflectance values are essentially insensitive to these two parameters for film thickness greater than ~ 2300 Å and evaporation pressures less than 8×10^{-8} Torr. Deposition rates were ~1000 Å/min.

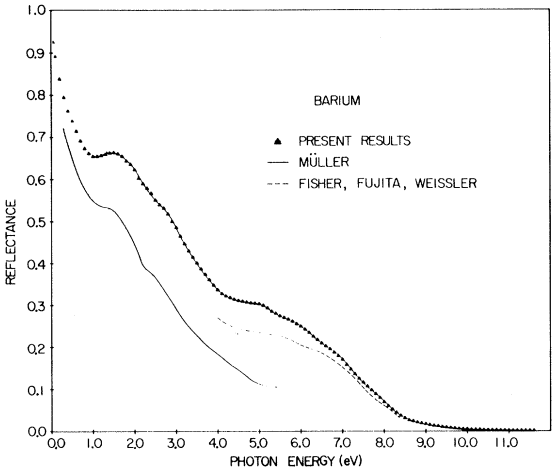

FIG. 6. Reflectance values of Ba as measured in the present study and as previously reported by Müller (Ref. 6). Also shown are the Ba uv reflectance measurements by Fisher *et al.* (Ref. 5). Reflectance values shown below the lower limit (1.0 eV) of the present study for Ba, as well as for the reflectance values for Sr, Eu, and Yb shown in the figures that follow, are part of the reflectance extrapolation used in the Kramers-Krönig analysis described in Sec. III.

surface roughness of 8-14 Å.

If one presumes that the film roughness is not appreciably worse than the roughness of the substrate on which it was grown (as is the case for most metals), then one can say according to the above measurements and theory that diffuse scattering from films grown on float-glass substrates is so small, even in the far uv, as to be unimportant. Coupling to surface losses should be minimal for the broad surface-loss functions encountered in the present materials (see Sec. III).

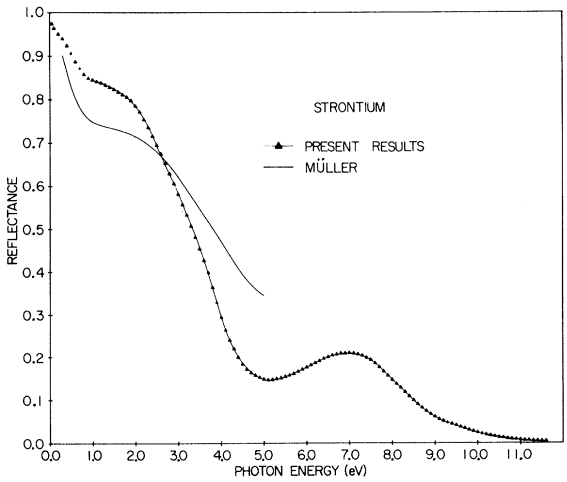

FIG. 7. Reflectance values of Sr as measured in the present study and as previously reported by Müller (Ref. 6).

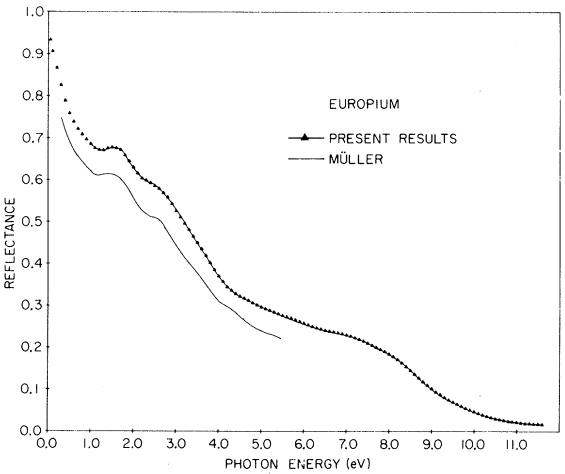

FIG. 8. Reflectance values of Eu as measured in the present study and as previously reported by Müller (Ref. 6).

The possibility that films grown on even very smooth substrates might have rough surfaces prompted a study of film growth versus thickness. A crystal oscillator was used to monitor the film thicknesses and reflectivities were measured for various thicknesses. The results of such measurements on Ba are shown on Fig. 5. The measurements gave no indication of surface deterioration with increased film thickness.

C. Reflectance

The results of the ultrahigh-vacuum free-surface near-normal incidence reflectance measurements on Ba, Sr, Eu, and Yb are shown in Figs. 6–9. Measurements were taken every tenth of an eV from 1.0 to 11.6 eV and are considered accurate to within ± 1.0% (measurements yielding reflectivities less than 10% are considered accurate to within a few tenths of a percent). Included on these figures are the reflectivity extrapolations below 1.0 eV which were used in the Kramers-Krönig inversion of the reflectivity data (Sec. III), and the results of Müller's reflectivity measurements on these materials.

Müller's reflectance measurements were undertaken along with transmission measurements to determine the optical constants directly from 0.3 to 5.0 eV. It is important to note that Müller's samples were prepared inside an ampoule having a sapphire window.[6] Films were evaporated on the inside of the sapphire window at an unspecified pressure, and the ampoule sealed off from the vac-

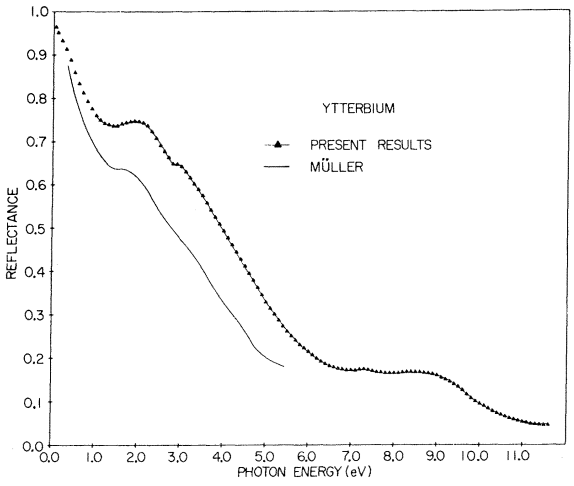

FIG. 9. Reflectance values of Yb as measured in the present study and as previously reported by Müller (Ref. 6).

uum system at an ultimate pressure of 10^{-8} Torr. Reflectance was then measured off the sapphire-metal interface using a reflectometer design described by Bennett and Koehler.[11] Müller's measurements were thus made under higher-pressure conditions; although it is felt that of possibly greater importance in explaining the large discrepancies in the absolute reflectance values between Müller's results and the present results is the fact that Müller's results were made at a sapphire interface with these highly reactive materials. Nevertheless, discrepancies in absolute reflectance should not obscure the fact that structure in the reflectance measurements of Ba, Sr, and Eu yielded excellent agreement with previous studies. Only Yb showed even a slight change in reflectance structure, the small enhanced shoulder appearing near 3.0 eV photon energy in the present result.

As an example of a second *free-surface*-reflectance measurement, we cite the results of Fischer *et al.*[5] for Ba (Fig. 6). They deposited their films very rapidly (~ 5 sec) at pressures which reached 10^{-5} Torr. It is interesting to note that their results are in much better agreement with the results reported in this paper than are Müller's. We feel that the remaining discrepancy with their results might be explained in terms of gas contamination.

III. KRAMERS-KRÖNIG INVERSION AND OPTICAL CONSTANTS

Reflectance from a metal-vacuum interface is a causal response, and as such its magnitude and phase are related by the well-known Kramers-Krönig integral.[20] This integral relating reflectance phase to reflectance magnitude extends over the entire frequency range, thus, it is necessary, in theory, to know the reflectance of the material at all frequencies. In reality, the reflectance of a material can often be extrapolated beyond the region of reflectance measurement without seriously affecting the accuracy of the reflectance-phase calculation within the frequency range for which measurements were made. Errors in the reflectance phase and in the optical constants calculated from the reflectance magnitude and phase still remain, however, and are primarily a result of, and sensitive to, the extrapolations of the reflectance data. For these reasons, it is desirable to discuss the schemes used to extrapolate our reflectance data below 1.0 eV and above 11.6 eV, and to derive a coarse estimate of the errors which these extrapolations introduce into the resultant optical constants.

A. Data Extrapolation

1. *Low-Frequency Extrapolation*

Although the absolute value of Müller's reflectance measurements were at variance with the results reported here, we noted above that the structure in Müller's results were well correlated with the structure in the present results. With this justification, the scaling of Müller's data was used to extrapolate our data from 1.0 down to 0.3 eV. The actual parameters which were scaled were $[1 - R(h\nu)]$ rather than $R(h\nu)$ for the respective experiments, since it was presumed that both Müller's results and the present results would converge to $R \simeq 100\%$ if the measurements had been carried to sufficiently low frequencies.

Data points for the Kramers-Krönig inversion extended to a minimum of 0.05 eV. Reflectance data between 0.05 and 0.30 eV were generated using the Drude model for the reflectance of a metal. Justification of this approach is somewhat tenuous; for although the optical constant $\epsilon_2(h\nu)$ should be unaffected by interband transitions for frequencies below the onset of such transitions, $\epsilon_1(h\nu)$ and thus the reflectance are affected by interband transitions even to lowest energies. The problem is compounded by the inability of unambiguously identifying the onset energy for interband transitions. Fortunately, the results of the Kramers-Krönig analysis are extremely insensitive to the precise extrapolation used to extend reflectance from a specified value at 0.30 eV to a value at 0.05 eV when subject to the additional constraint that R approach 100% as $h\nu$ approaches 0-eV photon energy.

Although the calculated optical constants were quite insensitive to the exact Drude reflectance

extrapolation used, concern over the free-electron or Drude optical constants will again emerge when discussing the interband contributions to the optical conductivity of each of the four materials (see Sec. IV). For this reason, it is useful to give a careful explanation of how the Drude curves were determined. The parameters which define the Drude absorption in a metal are the electron density n, optical mass m_{opt}, and scatter time τ. The electron density n is uniquely specified by the density and valence of the metal. A knowledge of the dc conductivity of the metal and the relation

$$\sigma_0 = ne^2\tau/m_{opt}$$

further reduces the number of free parameters to one, τ/m_{opt}. The optical masses of these materials have not been measured directly but a lower limit on their values may be attained by noting that for the divalent materials under study, the Fermi surface has considerable contact with Brillouin-zone faces. In this instance, Cohen[21,22] has shown that $m_{opt} \geq m_t$ where m_t is the thermal effective mass – a parameter which has been measured for all four materials.[21,23] The thermal effective mass was used in place of the optical mass in generating the optical constants and reflectivities of all four materials. Accurate dc conductivity values were available for Eu and Yb[24] and were used to calculate the dc scatter time τ_{dc}. The Drude reflectivity was then matched exactly to the reflectivity at 0.3 eV by linearly decreasing τ from its dc value as a function of energy. It was found that for both Eu and Yb the match with the 0.3-eV data occurred for a scatter time $\tau(0.3\text{ eV}) \cong 0.5 \times \tau_{dc}$. This necessity of tapering the scatter time from its dc value may, in fact, indicate a frequency-dependent scattering time such as has been observed in the alkali and other metals,[22] or it may indicate that interband excitations may occur at even the lowest excitation energies, such as occurs in aluminum, so that the pure Drude model for the metal is inapplicable. Reliable dc conductivity values were not available for Ba and Sr, and so values were arbitrarily selected which would give reflectance values that matched the reflectance data at 0.3 eV. For consistency, the same energy-dependent scattering-time taper [$\tau(0.3\text{ eV}) = 0.5\ \tau_{dc}$] used in calculating the Drude reflectance of Eu and Yb was used in this Drude model of the reflectance of Ba and Sr. All of the parameters used in calculating the Drude reflectance from 0.05 to 0.30 eV in the present reflectance extrapolation, and used in generating the Drude optical constants at all frequencies (see Sec. IV), are listed in Table II.

The numerical values for the entire low-frequency reflectance extrapolation, including both the scaling of Müller's data and the Drude reflectance values, are shown graphically in Figs. 6–9. An estimate for the percent error introduced into the optical constants because of inadequacies in the low-frequency extrapolation was achieved by doing a Kramers-Krönig analysis on one of the materials (Eu) using two different low-frequency extrapolations which formed reasonable maximum and minimum brackets on the tail actually used below 1.0 eV. The results of these calculations showed a spread in the values of ϵ_1 or ϵ_2 of ~± 20% near 1.0 eV. This spread decreased sharply at higher energies, and became negligible (< 1%) above 4.0 eV.

2. *High-Frequency Extrapolation*

While the procedure used in determining the high-frequency reflectance extrapolation is quite straightforward, errors introduced into the optical constants as a result of uncertainties in this extrapolation are considerably more serious than the errors introduced by uncertainty in the low-frequency extrapolation. While the effects of the low-frequency extrapolation on the optical constants died off at energies above 4.0 eV, the effects of varying the high-frequency extrapolation were appreciable at all frequencies. This sensitivity of the optical constants at all frequencies

TABLE II. Drude parameters used in generating the low-frequency reflectance tails for the Kramers-Krönig analysis of Sec. III. These parameters were also used in the interband conductivity calculations of Sec. IV. Also shown is a comparison of free-electron plasma energies calculated from the electron densities of the metals, and the energies of the experimentally observed loss-function peak positions (Sec. III C).

	Drude parameters				$\hbar\omega_p$ (eV) (Free-electron plasma frequency)	Experimental loss-function peak (eV)
	m_{opt}	τ_{dc} (sec)	N(cm^{-3})	σ_{dc} (sec^{-1})		
Ba	1.4	1.28×10^{-15}	3.18×10^{22}	0.737×10^{16}	6.62	7.33
Sr	2.0	7.64×10^{-15}	3.60×10^{22}	3.48×10^{16}	7.04	8.27
Eu	1.7	1.79×10^{-15}	4.16×10^{22}	1.11×10^{16}	7.57	8.66
Yb	2.0	5.18×10^{-15}	4.83×10^{22}	3.16×10^{16}	8.16	9.57

to the high-frequency tail means that a knowledge of reliable optical constants at any frequency may be used in determining the appropriate form for the reflectance tail. Such optical constants could conceivably be determined by independent ellipsometry or transmission-reflection measurements in a spectral range of easy measurement. Unfortunately, there are no reliable measurements of this type which are available for the materials under study, and thus a method of determining the high-frequency reflectance extrapolation was developed which was peculiarly suited to these metals. The method utilizes this sensitivity of the optical constants – particularly in the far-uv region – to the reflectance tail above 11.6-eV photon energy.

The plasma frequencies of all four materials studied lie considerably below 11.6 eV. Thus, the reflectance at these higher energies is quite small and the optical decay lengths quite large (see "opacity thickness", Table I, also Figs. 6–9). Consequently, the high-frequency reflectance of slightly transparent films of these materials is very sensitive to film thickness, Fig. 5. It is also sensitive to the optical constants of such materials. This high sensitivity to optical constants means, in turn, that a computer calculation of thin-film reflectance based on the optical constants calculated from opaque-film experimental reflectance and a high-frequency reflectance extrapolation will be quite dependent on the form of this high-frequency reflectance extrapolation. Since reflectance measurements can be made on films of known thickness with the aid of a crystal-thickness gauge, the reflectance extrapolation above 11.6 eV for an opaque film can be varied until the resultant thin-film computer reflectance agrees with the experimentally determined thin-film reflectance.

A simple single-parameter reflectance tail of the form ω^{-p} was used. The optical constants, and thus the computer-calculated thin-film reflectance, could then be varied by adjusting the single parameter p. In Fig. 10 we see an example of such a p-tail determination. The figure shows the experimentally observed reflectance of Eu for an 820-Å film, and an opaque film. Also shown are three computer calculations of the reflectance for 820-Å films characterized by the Eu optical constants resulting from three different p-value reflectance tails. One of the p values, called the "optimum" p value, yields the thin-film reflectance which is in good agreement with the experimental thin-film reflectance. The other two p values, $p+$ and $p-$, yield optical constants which are roughly 20% greater, and 20% less than the optical constants resulting from the "optimum" value. Both the optical constants and the size of

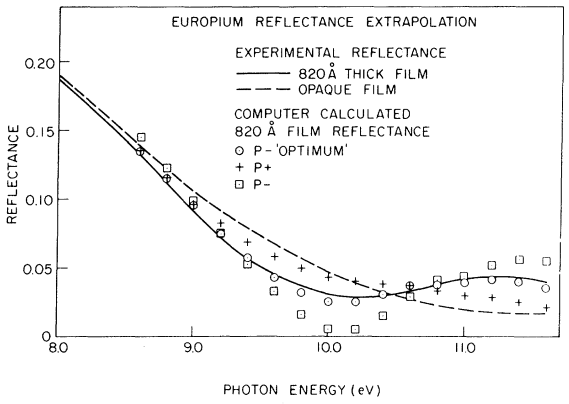

FIG. 10. Illustration of the method used to determine the high-energy reflectance extrapolations in the Kramers-Krönig analysis. The measured reflectance for a semitransparent film is fitted with thin-film reflectance values calculated with optical constants obtained from several different reflectance extrapolations above 11.6 eV (the extrapolations are indicated by $p+$, p_{opt}, and $p-$). As can be seen, the p_{opt} extrapolation gives a good fit. The $p+$ and $p-$ tail extrapolations yielded ϵ_2 values which were, respectively, 20% higher and 20% lower than the optical constants of the p_{opt} tail over the 8.0–11.6 eV spectral range shown.

the interference structure in the calculated thin-film reflectance vary monotonically with p, thus, p "optimum" is unique, and the uncertainty in the calculated optical constants can be related to the uncertainty in the determination of $p-$ "optimum." It can be seen from Fig. 10 that any ambiguities in the value of $p-$ "optimum" are well within the 20% error brackets defined by the $p+$ and $p-$ curves. The slight descrepancies which remain between the thin-film reflectance calculated from $p-$ "optimum" and the experimentally measured thin-film reflectance are primarily due to experimental nonuniformities in film thickness, limitations of a single-parameter reflectance extrapolation, and the use of pure quartz rather than float glass for the substrate optical constants needed in the thin-film computer calculation.

Uncertainty in the optical constants, arising from our inability to precisely specify the high-frequency tail, was within the 20% error brackets for the optical constants of Yb, Ba, and Sr as well as for Eu. Errors arising from the high-frequency tails actually drop below ±10% in the region below 4.0 eV where errors from the low-frequency tail prevail. Thus, inclusion of errors from both low- and high-frequency reflectance extrapolations yield optical constants for all four metals which should be accurate to ±20% over the entire spectral range of measurement.

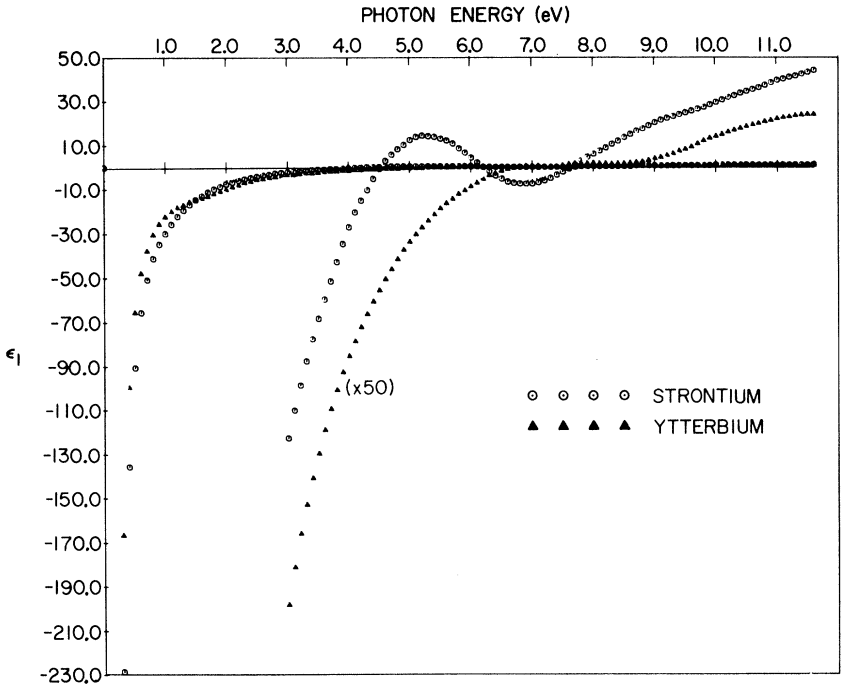

FIG. 11. Optical constant ϵ_1 obtained for the two fcc metals Sr and Yb.

B. Optical Constants

The complex dielectric constant, optical conductivity, and absorption coefficient, as calculated from a Kramers-Krönig analysis of our measured reflectance using the above extrapolation techniques, are shown for all four materials in Figs. 11–18. Stabilization or slight increases in the absorption coefficient and optical conductivity which appear above 11.0 eV in all four materials are probably a result of the discontinuity in the slope of the reflectance data at 11.6 eV – the onset of the high-frequency extrapolation. These optical

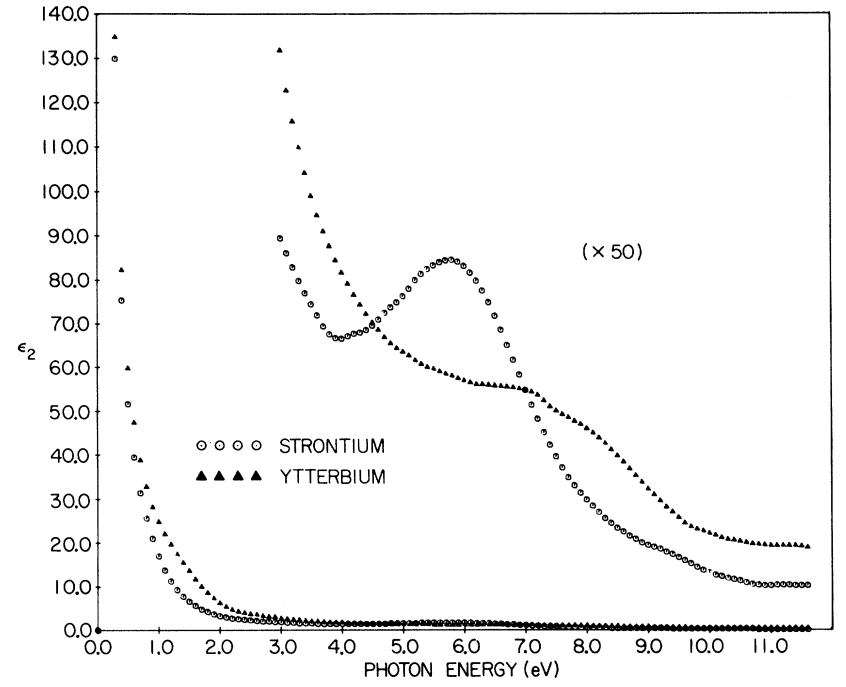

FIG. 12. Optical constant ϵ_2 obtained for the two fcc metals Sr and Yb.

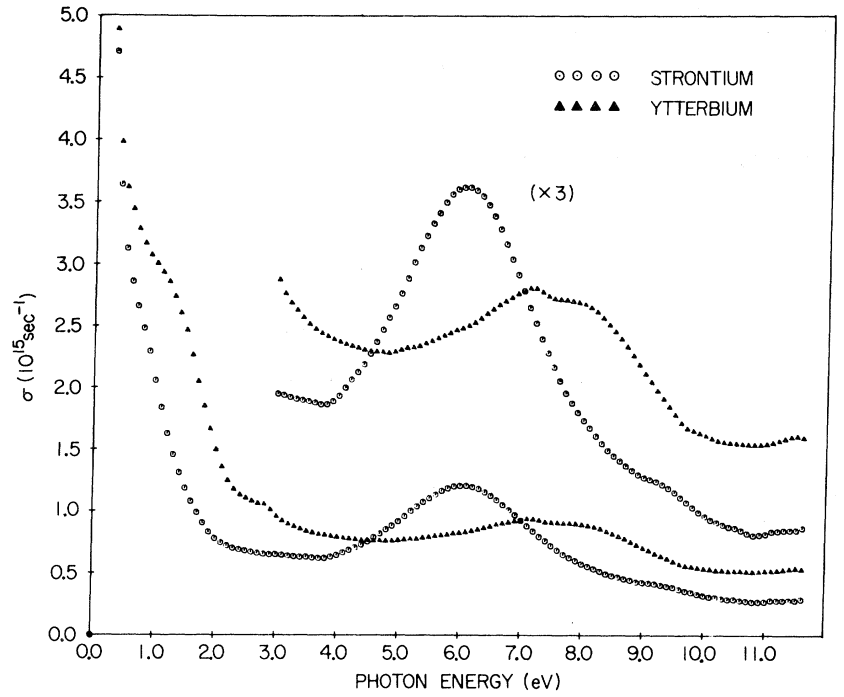

FIG. 13. Optical constant σ obtained for the two fcc metals Sr and Yb.

constants were calculated beyond 11.6 eV, and showed no larger structure which might be associated with this discontinuity. It was felt, however, that the optical constants above 11.6 eV were not particularly meaningful in view of the low reflectance and crude extrapolation technique in this region, and our data is thus terminated at 11.6 eV. The reflectance extrapolation below 1.0 eV was felt to have a strong enough physical and experimental justification to warrant inclusion of the calculated optical constants to 0.3 eV.

Confirmation of the estimated error in the ab-

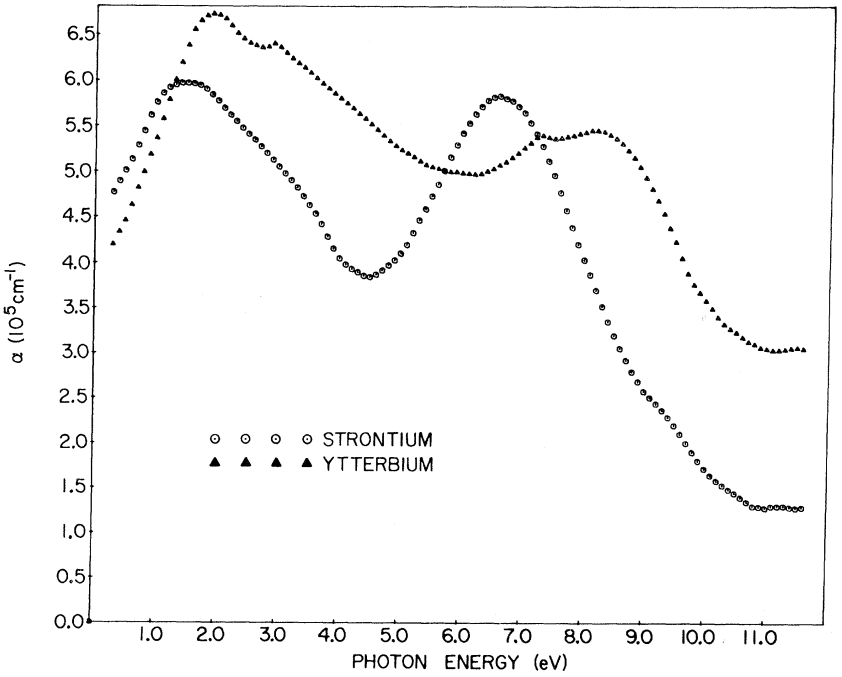

FIG. 14. Optical constant α obtained for the two fcc metals Sr and Yb.

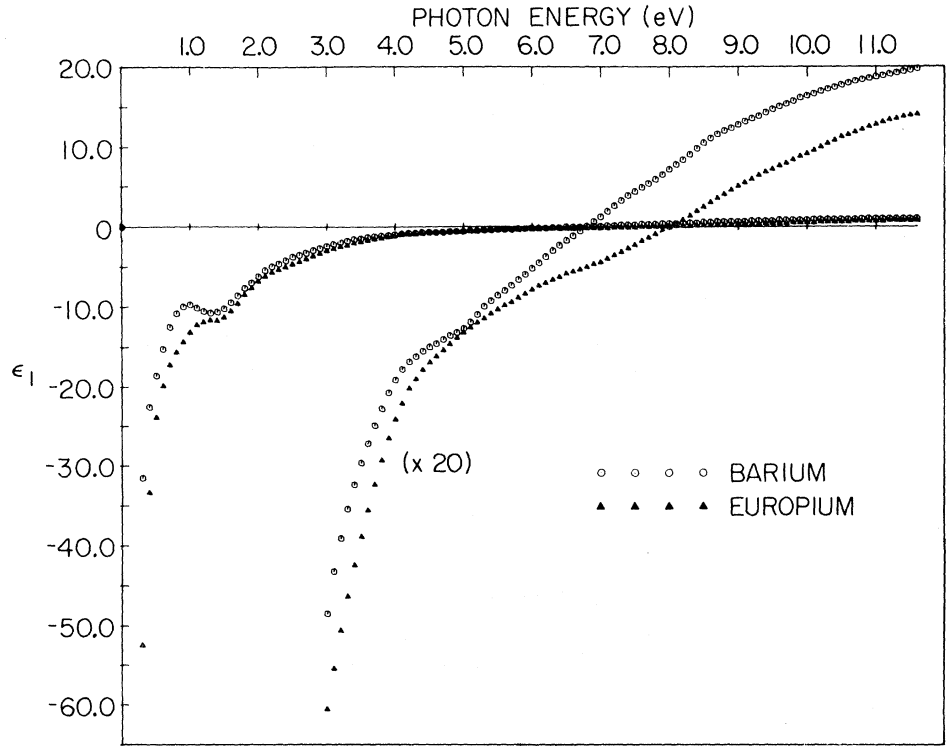

FIG. 15. Optical constant ϵ_1 obtained for the two bcc metals, Ba and Eu.

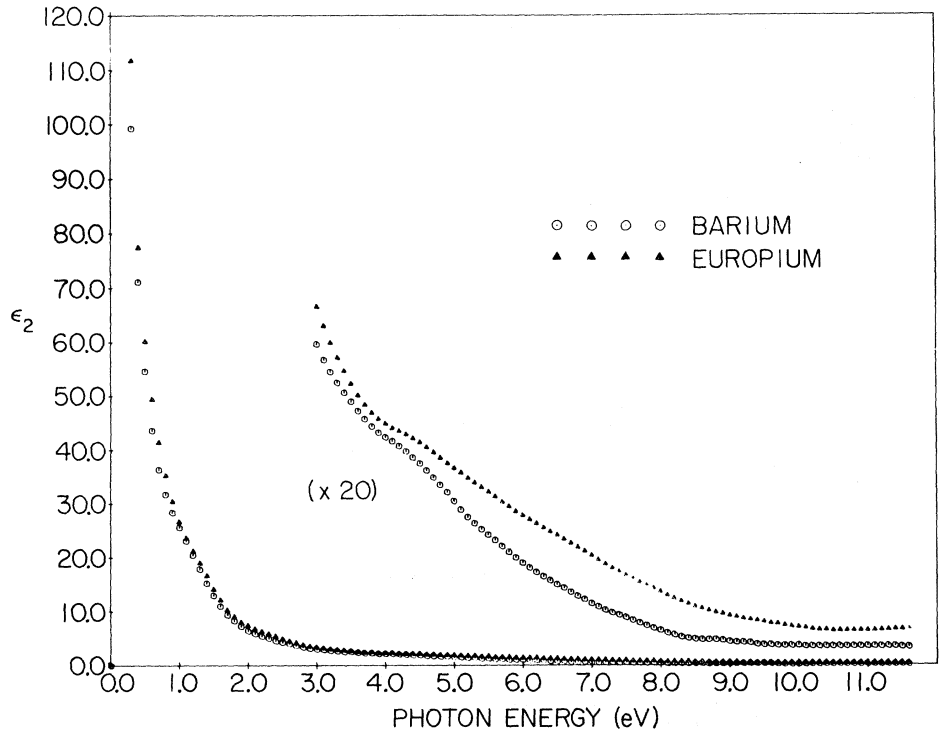

FIG. 16. Optical constant ϵ_2 obtained for the two bcc metals Ba and Eu.

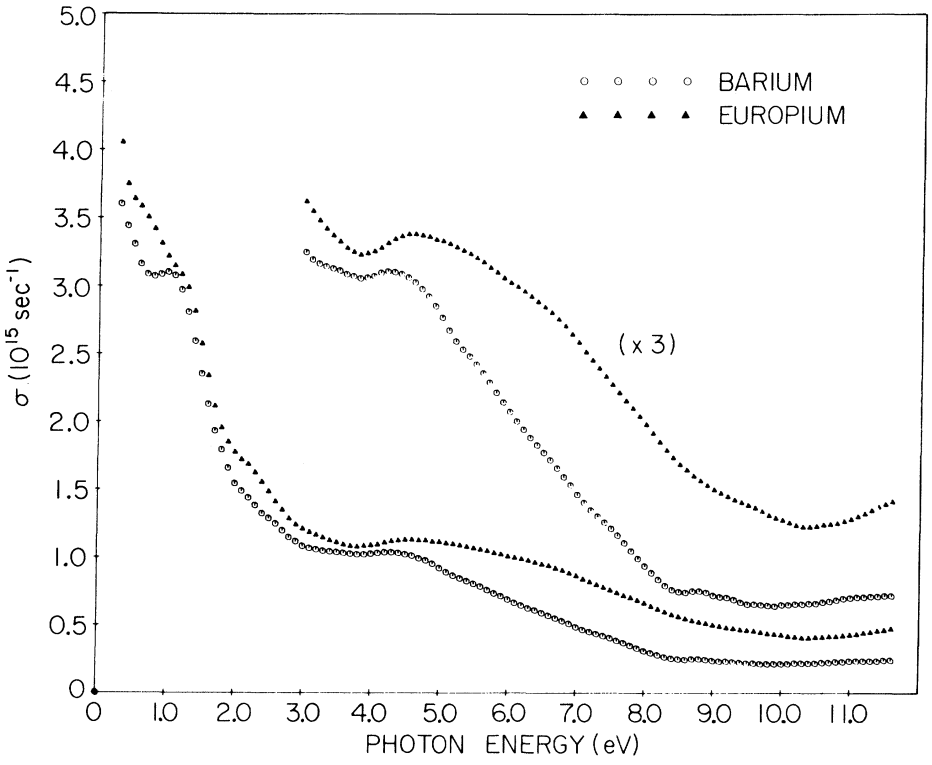

FIG. 17. Optical constant σ obtained for the two bcc metals Ba and Eu.

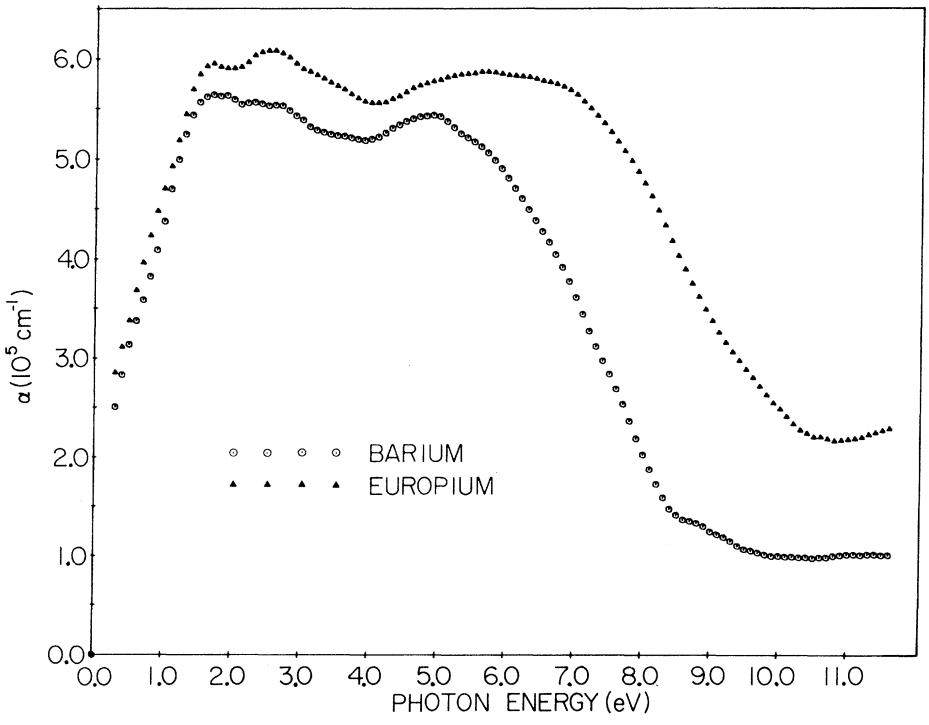

FIG. 18. Optical constant α obtained for the two bcc metals Ba and Eu.

solute accuracy of these optical constants may be gained through a comparison with optical constants of Ba calculated by Fisher *et al.*[5] and a comparison with peak positions in the volume-loss functions calculated in the high-energy electron-loss experiments by Kunz.[25]

The best previous free-surface measurement of the optical constants of any of the materials studied was carried out on Ba by Fisher *et al.* In that study, reflectance was measured at 65° as well as near-normal incidence, and from these data the optical constants n and k were determined for Ba. The results of that calculation are given in Fig. 19 for comparison with the optical constants of the present calculation. The divergence of the two results is greatest at low frequencies – the frequency range at which Fisher's near-normal incidence reflectance also has greatest divergence with the present result. Nevertheless, the agreement between Fisher's values for n and k and the independently calculated values of the present experiment are well within the estimated error limits of the optical constants reported in this article.

Further confirmation of the accuracy of the optical constants may be found by comparing the loss functions which are calculated from these optical constants in Sec. III C with loss functions determined from the high-energy electron-loss experiments by Kunz.[25] It was found that the uncertainty in the absolute value of our optical constants should result in an uncertainty in the peak position of the volume-loss function which is greater than ± 0.2 eV. Kunz's loss-function peaks were indeed within 0.2 eV of our calculated peak positions for both of the materials Ba and Sr studied by Kunz. This agreement may be seen in Figs. 20 and 21.

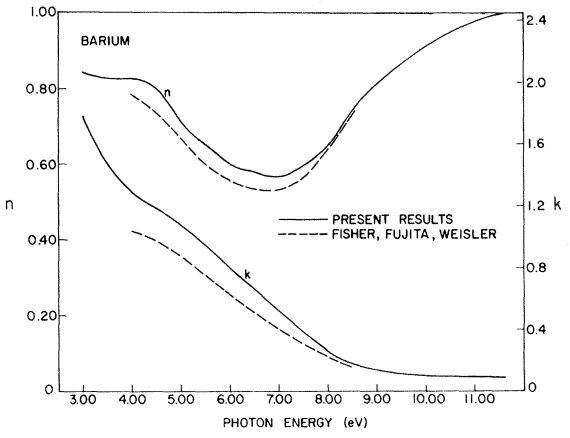

FIG. 19. Comparison of the optical constants n and k for Ba obtained in the present result with those obtained for Ba in a previous study by Fisher *et al.* (Ref. 5).

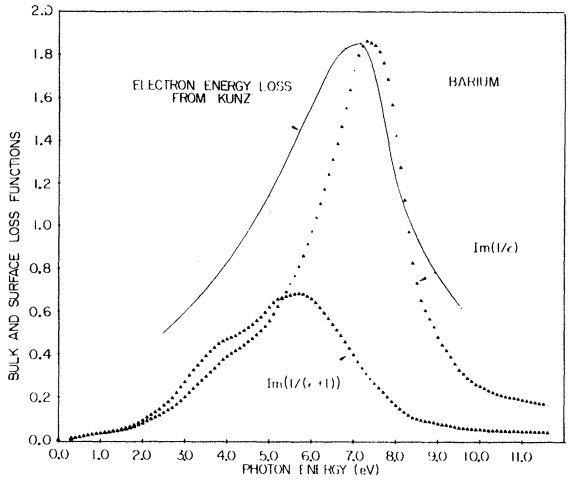

FIG. 20. Volume-loss function $\mathrm{Im}(1/\epsilon)$ and approximate surface-loss function $\mathrm{Im}[1/(\epsilon+1)]$ as calculated from the optical constants determined in the present study for the bcc metal Ba. Also shown is the volume-loss function of Ba as determined in high-energy electron-loss experiments by Kunz (Ref. 25).

C. Volume- and Surface-Loss Functions

The optical constants derived for the four metals under study were used to generate the volume- and approximate surface-loss functions for these materials. Arakawa *et al.*[26] have pointed out that loss functions determined in this manner are often superior to those determined in high-energy electron-loss experiments in that they yield a resolu-

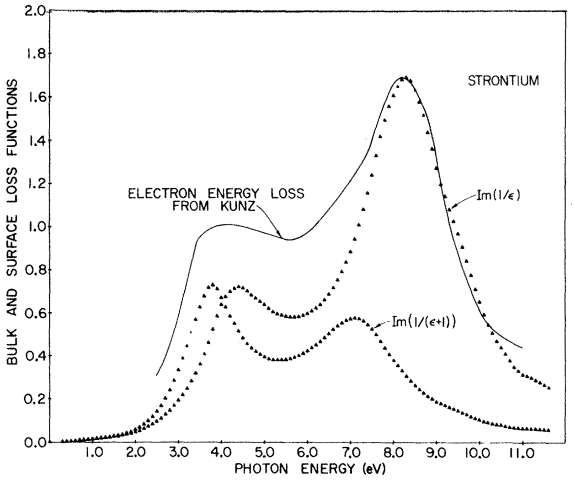

FIG. 21. Volume-loss function $\mathrm{Im}(1/\epsilon)$ and approximate surface-loss function $\mathrm{Im}[1/(\epsilon+1)]$ as calculated in the present study for the fcc metal Sr. Also shown is the volume-loss function of Sr as determined in high-energy electron-loss experiments by Kunz (Ref. 25).

tion and allow a separation of volume- and surface-loss effects which is often quite difficult to achieve in the electron-loss experiment.

The loss functions for the two bcc metals are given in Figs. 20 and 22, while those for the fcc metals are shown in Figs. 21 and 23. Also shown on the alkaline-earth loss-function plots are the volume-loss functions measured by Kunz [25] in his high-energy electron-loss experiments on these two metals. The experimental volume-loss-function peak positions are listed in Table II for comparison with the free-electron plasma energies.

The function plotted for the surface-loss function is $\mathrm{Im}[1/(\epsilon+1)]$. This is an approximate expression to the surface-loss function first derived by Ritchie [27] but Arakawa [26] has noted that this function yields the essential features of the exact expression.

What is probably the most interesting aspect of these loss-function plots is the presence of two prominent pieces of structure in the loss functions of each of the two fcc metals. This effect is most prominent in Sr where both the surface- and volume-loss functions each exhibit two distinct peaks. These two pieces of structure were first observed by Kunz. [25] The effect is a direct result of the triple zero crossing experienced by ϵ_1 for the two fcc metals and seen quite graphically for Sr in Fig. 11. The triple crossing of ϵ_1 for Yb is not obvious from Fig. 11, but does indeed occur, resulting in a peak and a shoulder for the surface- and the volume-loss functions of Yb.

It should be noted that the loss functions of all four of these metals show an appreciable broadening which is characteristic of materials having a

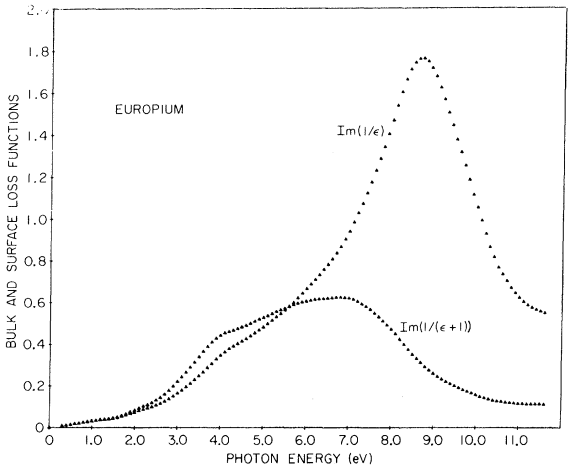

FIG. 22. Volume-loss function $\mathrm{Im}(1/\epsilon)$ and approximate surface-loss function $\mathrm{Im}[1/(\epsilon+1)]$ as calculated in the present study for the bcc metal Eu.

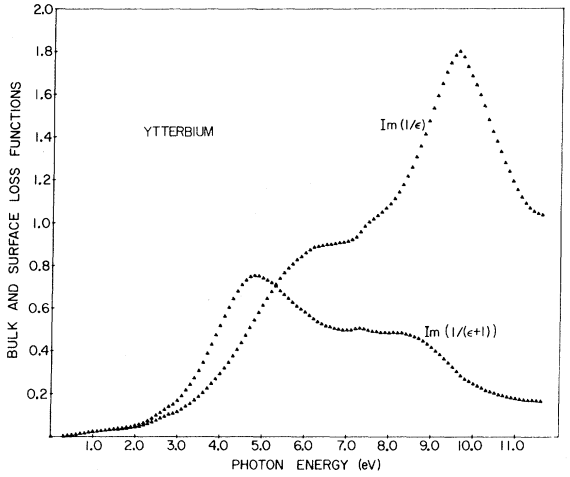

FIG. 23. Volume-loss function $\mathrm{Im}(1/\epsilon)$ and approximate surface-loss function $\mathrm{Im}[1/(\epsilon+1)]$ as calculated in the present study for the fcc metal Yb.

relatively large density of interband transitions near their collective oscillation frequencies. [26] The strength of such interband transitions in these materials is pursued in Sec. IV.

A comparison of the loss functions calculated for the two alkaline-earth metals and those measured on these same materials by Kunz yields an agreement which is striking in comparisons of data of this type. The dominant peak positions of 7.33 eV for Ba and 8.27 eV for Sr were quite close to the peak positions of 7.1 eV for Ba and 8.1 eV for Sr observed by Kunz. The implications which this agreement has on the accuracy of our optical-constant calculation has been discussed.

While the uncertainty in our volume-loss-peak positions was estimated from the uncertainty in the value of our optical constants, no such uncertainty in the shape of the calculated loss functions was estimated. It is, thus, possible that the discrepancies between the shapes of Kunz's loss functions and those reported in the present paper result from uncertainties in the optical constants used to calculate the present functions. However, the fact that the discrepancies are strongest on the low-frequency side of the loss functions where the error in the optical constants arising from the reflectance extrapolation is minimal would cast some doubt on this possibility.

As has been mentioned, Arakawa [26] has pointed out that it is often quite difficult to separate the effects of surface and volume losses in a high-energy electron-loss experiment. This results primarily from surface preparation and experimental angular-resolution problems. [27] It is interesting to note in this regard that substantially

improved agreement can be obtained between Kunz' s measured loss function and the present results by plotting the volume plus 1.25 × the surface-loss functions calculated in the present result against Kunz's loss functions. The same ratio of volume-to-surface-loss functions was used for each metal, and the resultant improved agreement was much the same for each metal as can be seen in Fig. 24.

IV. INTERPRETATION OF OPTICAL PROPERTIES

A. Crystallographic versus *f*-Electron Effects

Separation of the crystallographic and possible *f*-electron effects is central to the purpose of this study. A more quantitative analysis of the physical origins of the optical constants described in Sec. III is given in Sec. IV B. However, we want first to emphasize the most obvious and striking qualitative features of comparing the calculated optical constants of those metals sharing a common crystal structure, and of those rare-earth metals sharing partially filled or filled 4*f*-electron shells.

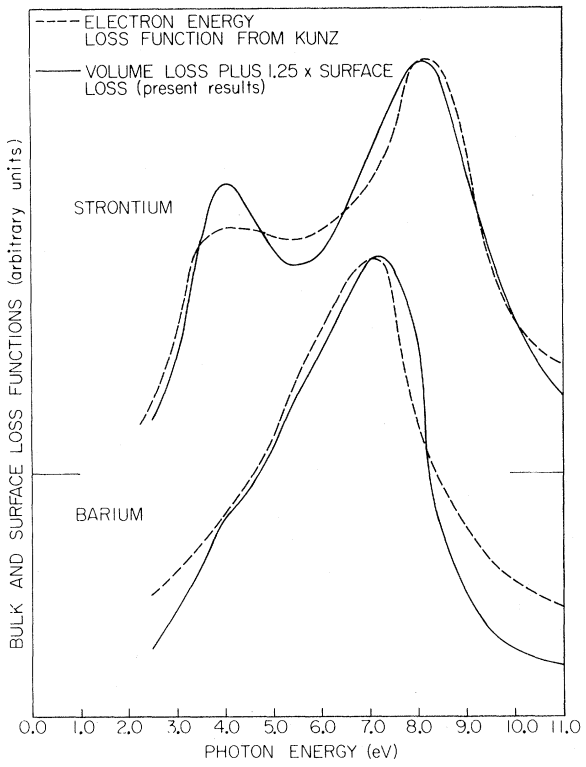

FIG. 24. Comparison of the volume-loss functions determined from Kunz's high-energy electron-loss experiments on the alkaline earths Ba and Sr, with a weighted average of the volume- and approximate surface-loss functions determined for Ba and Sr in the present study.

1. *Crystal Structure*

The strong correlation between the optical constants of materials sharing a common crystal structure is immediately obvious in comparing the constants derived for fcc Sr and Yb presented in Figs. 11–14, and in comparing the constants derived for bcc Ba and Eu as shown in Figs. 15–18. Of particular interest is the prominent piece of structure in the optical conductivity which occurs in the uv region of all four metals. This structure is somewhat stronger and occurs at noticeably higher energies in the fcc structures of Sr and Yb than in the bcc crystal structures of Ba and Eu. It has been mentioned in Sec. III that the structure is in fact strong enough to cause a triple rather than a single zero crossing of ϵ_1 in both fcc materials. The structure in σ for the bcc materials is less strong, and ϵ_1 for these metals increases monotonically as one might expect for a metal.

A detailed comparison of the structure in these metals is obscured by the different energy scales of the observed optical properties. We refer in this regard to effects arising solely from the differing electron densities of the materials. Comparison of structure at lower energies is further hampered by the rapidly varying free-electron or Drude contribution to the optical constants. In order to make a more meaningful comparison, an attempt has been made to subtract out the Drude contribution to the optical conductivity, and the resultant plots of interband σ have been plotted against frequency normalized to the free-electron plasma frequency of the metal under study. The parameters used in determining the Drude contributions to σ and in normalizing the energy scale against which σ is plotted are all given in Table II and/or explained in Sec. III. $\tau = \tau(0.3\ \text{eV})$ is taken as the appropriate Drude scattering time at all energies greater than 0.3 eV. The actual plots of interband conductivities are shown paired according to crystal structure in Fig. 25.

It should be noted that while the Drude parameters used in deriving the interband σ are not particularly reliable (see Sec. III), the reliability of the resultant interband σ is affected only at lowest energies. Drude contributions to the optical constants in the uv are insignificant regardless of the Drude parameters used, and even at lower energies the lack of structure in the Drude σ affects the magnitude rather than shape or position of structure in interband σ. Thus, the position of all the structure shown in Fig. 25 is considered reliable to within ± 0.1 eV, while the magnitude of the structure in the uv is felt to be as reliable as

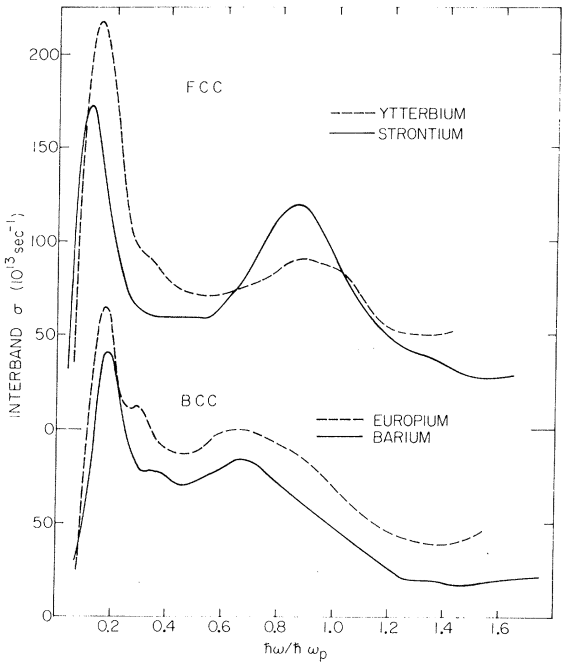

FIG. 25. Comparison of the "Drude-corrected" or interband optical conductivities for the two fcc metals Sr and Yb, and the two bcc metals Ba and Eu. Conductivities are plotted versus $\hbar\omega$ normalized to the free-electron plasma energy in order to eliminate variations in structure arising from differences in electron density.

the uncorrected optical σ from which it was derived.

Two important points should be obvious from the interpretation of Fig. 25. The first is that the correlation in σ between metals of the same crystal structure, first observed in the studies of these metals by Müller from 0.5 to 5.0 eV,[6,7] has been confirmed over this same spectral range in the present study. As will be mentioned in Sec. IV B, Table IV, it is the dependence of σ upon crystal structure that has been confirmed rather than the exact position and magnitude of structure in σ observed by Müller. We note in Fig. 25 that the positions of the peaks in the magnitude of σ just above the onset of interband transitions occur within less than 2% ω/ω_p of each other for the two bcc metals. There is also a second smaller piece of structure at slightly higher energies in both bcc materials. Peaks in σ near the onset of interband transitions in the fcc metals are not as well correlated with each other although both peaks occur at noteably lower energies than the onset peaks of the bcc metals. The only piece of structure in this spectral range studied by Müller which can not be correlated to crystal structure is the slight shoulder in interband σ occurring near 0.32 ω/ω_p in Yb, but not observed at a comparable energy in fcc Sr.

The second important observation which one can make from an interpretation of Fig. 25 is that the observed dependence of optical properties upon crystal structure at lowest energies may be extended into the far uv as a result of the present study. The large pieces of structure in σ which were shown in Figs. 13 and 17 and interpreted as being dependent on crystal structure are quite obviously directly related to crystal structure when plotted versus ω/ω_p. Differences in the positions of the fcc and bcc uv peaks in σ are significantly greater than the barely discernable differences in peak positions of metals having the same crystal structure.

2. 4*f* Electrons

The lack of any conclusive evidence for transitions from the 4*f* electrons in Eu and Yb must be considered as important a result of the interpretation of Fig. 25 as is the strong evidence for the correlation of structure in interband σ to crystal structure.

It was mentioned in the Introduction that there is strong reason to believe that the 4*f*-electron levels in Eu and Yb lie significantly less than 11.6 eV below the Fermi level. This assumption has in fact been confirmed in recent soft x-ray photoemission studies (ESCA) of Eu and Yb carried out by Brodén, Hagström, Hedén, and Norris.[28] Their results indicated transitions were occurring from what they believed to be 4*f* states lying between 2.0 and 3.0 eV below the Fermi level of both of these metals. Yet an examination of the interband conductivities of Fig. 25 yields no structure which might be unambiguously attributed to transitions from these 4*f* electrons. It is true that slight pieces of structure in σ do occur in the spectral range from 2.0 to 3.0 eV in both Eu and Yb, but such structure also occurs in Ba, and the assignment of this structure to transitions from 4*f* electrons becomes even more questionable when we note its sharpness and compare this with the gradual onset that one might expect of transitions from the *f*'s.

In order to see if there was any evidence of additional oscillator strength in the optical transitions from Eu and Yb which could not be detected in the structure appearing in Fig. 25, the extinction-coefficient sum rules were plotted for all four metals out to 11.6 eV. The sum rules are plotted versus ω/ω_p and shown together for easy comparison in Fig. 26.

The slight differences which do exist between the saturated sum-rule values shown in Fig. 26 are well within the experimental error for the ab-

solute value of the optical constants found in this study. Even if we were to believe these differences, there is no correlation between the differences and the presence or absence of $4f$ electrons.

One final point should be made with regard to the sum rules shown in Fig. 26. It is noted that the sum rules of all four metals saturate to a number greater than the 2.0 valence electrons for each of these four materials. It is well known that the sum rule of a material will approach a value greater than the number of its valence electrons if it has core states at energies reasonably close to the valence-state energies. This increase in the sum rule occurs even below the energy for the onset of transitions from the high-lying core states. For the case at hand, Ba, Eu, and Yb should all have filled $5p^6$-core states lying somewhere from 20 to 25 eV below the Fermi level.[3] Sr has a filled $4p^6$ shell lying at approximately the same energy below E_F. These core levels are sufficiently close to the Fermi level to explain the values attained by the sum rules. It should also be noted that the presence or absence of $4f$-core states should not affect the sum rules in this indirect manner to the same extent as the $5p$-core states. The important coupling parameter in this discussion is the matrix element coupling the core state and the *filled* valence state. Since the filled valence states of these metals should be quite s-like, matrix-element coupling should be appreciably stronger with the $5p$-core states than $4f$-core states.

We must conclude from our preceding discussions that there is little conclusive evidence for transitions from $4f$-electron states of Yb and Eu either in anomalies in the structure of the optical conductivity or in increased oscillator strength in materials having $4f$ electrons.

This apparent paradox between the results of the present study and the observation of $4f$ transitions in soft x-ray photoemission by Brodén *et al.*[28] may possibly be best explained in a recent survey paper on the spectral distribution of atomic-oscillator strengths by Fano and Cooper.[29] Simply stated, we know that transitions from f states can only occur to states having "d" or "g" symmetry. The lowest unfilled states of d symmetry in Eu and Yb are known to occur within a few volts of the highest filled states of these metals for both the atomic and crystalline forms (see $5d$-electron effects in Sec. IV B. On the other hand, the lowest possible "g"-symmetry atomic state is the $5g$ state whose energy is undoubtedly above the spectral range of the present measurements. The $5g$ energy levels are probably not appreciably shifted in forming crystalline Yb and Eu. Thus, the only $4f$ transitions which should be observable in the present study are transitions to $5d$-like states. The important point is that Fano and Cooper have pointed out that oscillator strengths for a transition from a state with energy quantum number n to a state with energy quantum number n' which increases its angular momentum by one is roughly ten times as strong as a transition between the same two energy quantum states which decreases its angular momentum by one,[29,30] that is,

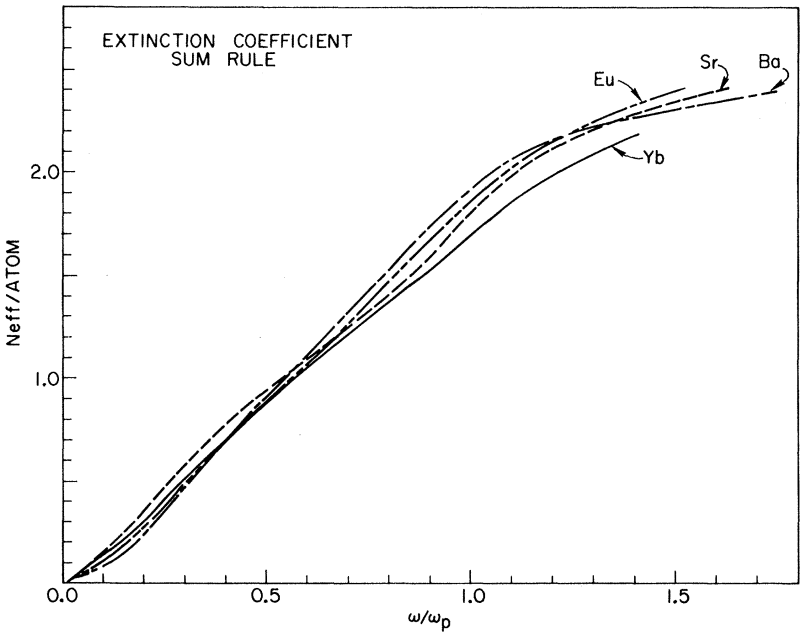

FIG. 26. Extinction-coefficient sum rules in effective number of electron per atom for Ba, Sr, Eu, and Yb, plotted versus $\hbar\omega$ normalized to free-electron plasma energies as in Fig. 25.

$$f(n, l \rightarrow n', l+1) \approx 10 \times f(n, l \rightarrow n', l-1).$$

One may thus inductively reason that the total $4f$ to d symmetry-state oscillator strength over all frequencies accounts for less than 10% of the total $4f$ to g symmetry-state oscillator strength over all frequencies. Transitions to the $5d$ states observable within the spectral range of the present study must thus account for significantly less than 10% of the total transition strength to all final states of d and g symmetry. This preference for higher angular momentum in the excited state is physically justified by noting that when an electron moving in an orbit increases its energy, it prefers to also increase its angular momentum.

It should be made clear that the above discussion has assumed that the atomic-oscillator strengths for various $4f$ transitions in Eu and Yb remain qualitatively unchanged in going from the atomic to crystalline state. This is a reasonable assumption for the rather tightly bound d, f, and g symmetry states considered. The atomic nature of the $l \geq 3$ states in the crystalline forms of the rare-earth metals is in contrast with the strong perturbation of the $6s$ atomic valence electrons which occurs in forming the crystalline state. It is a combination of this strong crystalline perturbation of the $6s$ electronic states and an anomalously high $6s \rightarrow 6p$ oscillator strength [31] which causes the $6s$ oscillator strength to saturate to two electrons/atom within the spectral range of the present study as was seen in Fig. 26. It is against this very strong $6s$ oscillator strength that the $4f$ absorption must be observed.

If one makes the rather severe assumption that half of the total oscillator strength associated with the $4f \rightarrow d$ transitions is included in the $4f \rightarrow 5d$ transitions, then these transitions would contribute at most 5% of the total $4f$ oscillator strength, or 0.35 electrons/atom for Eu and 0.70 electrons/atom for Yb. One would, in fact, expect the $4f \rightarrow 5d$ transitions to contribute considerably less than one-half of the total strength for $4f \rightarrow d$ transitions, [32] so that the contribution of the $4f \rightarrow 5d$ transitions should be noticeably less than 0.3 electrons/atom in Eu, or 0.70 electrons/atom in Yb.

This picture is not inconsistent with recent theoretical band calculations [33] and photoemission studies on the Eu calcogenide insulators, [34,35] which have indicated that total contributions to oscillator strengths for transitions from the half-filled Eu $4f$ shell in the calcogenide band gaps to $5d$ band above the conduction-band edge are down from the transition strengths from valence band to conduction band by well over an order of magnitude.

One conclusion that one draws from the above discussion is that oscillator strength arising from $4f$ transitions in Yb should be twice as great as in Eu, and according to the above discussion should be marginally observable in the present study even for reasonably small estimates of the $4f \rightarrow 5d$ transition strength. This may support an interpretation of the weak piece of structure appearing near 2.5 eV in fcc Yb but not observed in fcc Sr as being due to an onset of $4f \rightarrow 5d$ transitions. Evidence for this interpretation is not, however, supported by the Yb extinction-coefficient sum-rule calculation.

One final point should be mentioned with regard to transitions from $4f$ electrons in Eu and Yb. Fano and Cooper have pointed out that onsets of transitions to high-l-value continuum states are appreciably suppressed near threshold by the centrifugal barrier associated with $l \geq 2$ states. Such effects should cause a significant shift to higher energies of the threshold energy for the onset of $4f$ transitions to continuum d and g states in atomic Eu and Yb. The question arises as to whether this centrifugal barrier might not also cause a suppression of transitions to the "quasi-continuum" d and g bands which arise from the discrete atomic d and g levels in the formation of crystalline Eu and Yb.

The importance of the centrifugal barrier in suppressing the threshold of transitions to continuum states in atoms can be seen in Fig. 27. Shown are the calculated [36] and observed [37] absorption cross sections for the onset of transitions from the $4f$ states in gold to the continuum g states in gold. While the threshold first appears near 50 eV in the theoretical calculation, the absorption does not rise steeply enough to be experimentally detected

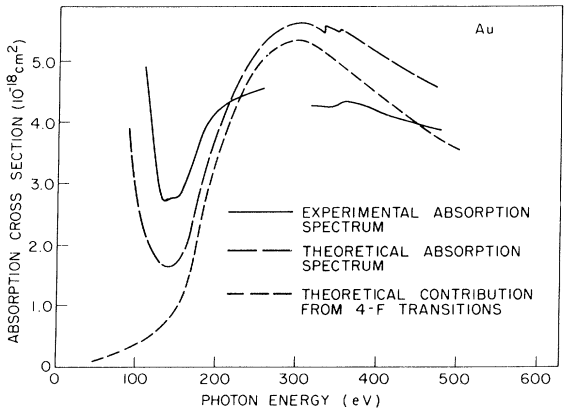

FIG. 27. Theoretical and experimental absorption cross sections for gold showing the centrifugal barrier suppression of oscillator strength in the photon-energy range between the $4f$-electron shell threshold near 50 and 100–150 eV.

until excitations of well over 100 eV are achieved. Such shifts in the effective thresholds of transitions to d continuum states also occur, although the magnitudes of such shifts are generally less than 10 eV. The effect, if any, which this centrifugal barrier has in suppressing transitions to d- and g-derived bands of Eu and Yb is part of the general and complicated problem of determining the perturbations of atomic potentials and wave functions in going to the crystalline state.

B. Origins of Interband Conductivity

As mentioned in Sec. I, recent band-structure calculations indicate the materials under study are not nearly-free-electron-like, but do, in fact, have strong d-electron effects in the energy range above the Fermi energy. Nevertheless, it is extremely useful to calculate the interband conductivity in the nearly-free-electron model so that major pieces of structure which cannot be explained in terms of this model may be identified and associated with effects such as d-band mixing or d hybridization which go beyond the simple free-electron model. In the section on the nearly-free-electron theory which follows, theoretical expressions for the interband conductivity are compared with observed interband σ for typical fcc and bcc metals. In Sec. IV B 2 an attempt is made to explain those pieces of structure which cannot be explained in the nearly-free-electron theory in terms of d-electron effects predicted by recent band calculations.

1. *Nearly-Free-Electron Theory*

The main assumptions in the nearly-free-electron theory of optical conductivity are first, that the energy bands are distorted from free-electron bands only in the regions near the Brillouin-zone faces, and second, that the distortion of the free-electron wave functions (or pseudo-wave-functions) which results from interaction with various Bragg reflection planes is so small that the contributions of the various Bragg reflection planes to the interband conductivity may be considered individually. The interband conductivity associated with each reciprocal-lattice vector may thus be calculated, and the total contribution to interband σ found by summing all lattice vectors contributing to σ over the energy range studied.

When the onset of transitions resulting from the interaction with a given Bragg reflection plane occurs near the center of the Brillouin zone (where the bands may be assumed undistorted from free-electron bands), the onset frequency may be obtained directly from the free-electron bands, and the exact form of the contribution of this Bragg reflection plane to σ may be found in the well-known theory of Wilson. [38] The only free parameter in this theory is $|V_G|$, the G Fourier component of the potential, where G is the reciprocal-lattice vector associated with the Bragg reflection plane under consideration.

When the onset of transitions occurs near a Brillouin-zone face, the free-electron bands may no longer be considered undistorted. The distortion of these bands is significant in comparison with the onset energy only in the case for which the final band is near the Fermi energy. Quite often the distortion of bands which meet these criteria results in a band splitting at the zone face with the Fermi level between the bands. The contribution of such a Bragg reflection plane to the optical conductivity has been extensively discussed in the theory of Golovashkin *et al.* and Harrison. [39] The onset frequency in this theory is no longer determined from the free-electron bands, but is directly related to the pseudopotential component $|V_G|_{psd}$ appearing in the theory. A second free parameter, a phenomenological lifetime, is also included in Golovashkin's theory in order to eliminate the singularity which would otherwise occur in σ at the zone face.

A calculation of interband σ in the nearly-free-electron model is thus reduced to a determination of the appropriateness of Wilson's or Golovashkin's theory and an evaluation of $|V_G|$ or $|V_G|_{psd}$ and lifetime broadening for each of the Bragg reflection planes contributing to σ over the spectral region of interest. Golovashkin's theory predicts that the energy of the peak position of a Bragg plane's contribution to interband σ is equal to the band splitting and related to $|V_G|_{psd}$ for that Bragg reflection plane. Golovashkin's theory will thus be applicable to any Bragg reflection plane for which an energy or band splitting equal to a known peak position in experimental σ yields a lower band which lies below E_F, and an upper band which lies above E_F. The sharp onsets of interband transitions which were observed in all four metals are suggestive of the sharp onsets predicted in Golovashkin's theory, and, in fact, there was at least one Bragg reflection plane for each metal which satisfied the criterion of Golovashkin's theory for band splittings given by these onset structure peak positions. Contributions to σ arising from these Bragg reflection planes were calculated in Golovashkin's theory with pseudopotentials and lifetime broadening determined from experiment in the manner described in the literature. [39] Although our above criteria for a Golovashkin-type transition could be satisfied by both the (200) and (1 1 1) Bragg reflection planes in our fcc metals, a Golovashkin-type contribution to σ was calculated only for the arbitrarily selected (200) plane, consistent with our observation of only a single sharp

onset in the two fcc metals. Golovashkin-type onsets were possible from only a single Bragg reflection plane in the two bcc metals. Contributions to σ from the remaining Bragg reflection planes capable of contributing to σ over the spectral range of interest were calculated in the theory of Wilson. Potential Fourier components $|V_G|$ for these planes were chosen to give best agreement with experiment consistent with reasonable magnitudes for the $|V_G|$.

A listing of all critical parameters involved in calculating contributions to σ from various Bragg reflection planes in the theory of Wilson or Golovashkin is included in Table III. Parameters fixed by the free-electron bands or crystal structure are listed, as well as parameters $|V_G|_{psd}$ and lifetime broadening γ that have been fitted to the experimental data in the manner described above.

In completing this discussion of the calculated interband optical conductivity in the nearly-free-electron model, it should be mentioned that theoretical $|V_G|_{psd}$ values determined by Animalu and Heine[40] are available only for Ba. Use of these values in the Golovashkin theory yields extremely poor agreement with the experimentally determined σ for Ba, and a comparison of these results has been omitted owing to the questionable reliability of these $|V_G|_{psd}$ values.

It was seen in Fig. 25 that there is a strong correlation of structure in optical σ to crystal structure. Theoretical peak magnitude values in the interband σ calculated in the theory of Golovashkin for the lowest-lying interband transitions are listed for these two bcc metals and two fcc metals in Table III. These values confirm that structure calculated in the nearly-free-electron model is also strongly correlated to crystal structure. The comparison of our theoretical and experimental interband optical conductivities is thus made for only a single fcc material Sr and single bcc material Eu. These values are shown plotted on a common scale in Fig. 28.

It can be seen that in the energy range below 4.0 eV, the nearly-free-electron model for optical σ gives reasonable agreement with the optical conductivity observed in the fcc metals. The onset energy and shape of the onset structure were, of course, fitted to the experimental curve, but the magnitude of the theoretical peak is in reasonable agreement with the magnitude of the experimental peak. There is no evidence in the observed conductivity of Sr for the existence of the slight piece of predicted structure associated with the (111) Bragg reflection plane. In the two bcc metals there are 12 rather than 6 physically equivalent Bragg reflection planes associated with the lowest-lying onset, and thus the magnitude of the theoretical peak in σ is quite large. The resultant agreement between the magnitudes of these experimental and theoretical lowest-lying peaks in σ is extremely poor. This lack of agreement is compounded by the inability of the nearly-free-electron model to explain the second piece of structure observed just above the onset of transitions ($\sim$2.5 eV in Eu, Fig. 28) in both bcc materials.

While the nearly-free-electron model is partially successful in describing the observed interband conductivity in the fcc metals below 4.0 eV, it is totally unable to account for the magnitudes, shapes, or positions of the prominent pieces of structure in σ found in all four materials at frequencies above 4.0 eV. While the magnitude of the theoretical σ could be adjusted by using unreasonably large values for $|V_G|$, there is no possible way that the onset frequencies determined from the free-electron band structure could be brought into agreement with the positions of these ob-

TABLE III. Parameters used in the nearly-free-electron optical σ calculation. The energy range over which transitions are possible in the Wilson theory ($h\nu_{min}$ to $h\nu_{max}$, as in Ref. 38), as well as the phenomenological lifetime broadening γ in the theory of Golovashkin *et al.* (Ref. 39) are presented. $|V_G|_{(psd)}$ values used in both theories are specified, and the values of the most prominent pieces of structure in the optical σ, occurring at lowest frequencies and described in the theory of Golovashkin *et al.* are also given.

Reciprocal-lattice vector G	n_G	Type of transition	Wilson parameters $h\nu_{min}$(eV)		$h\nu_{max}$(eV)		Golovashkin γ (eV)		$\lvert V_G\rvert_{(psd)}$ (eV)		Golovashkin σ_{max} 10^{13}sec^{-1}	
fcc			Sr	Yb	Sr	Yb	Sr	Yb	Sr	Yb	Sr	Yb
(200)	6	Gol.	•••	•••	•••	•••	0.32	0.49	0.39	0.57	224	258
(111)	8	Wil.	1.63	1.96	26.5	31.9	•••	•••	0.65	0.65	•••	•••
(220)	12	Wil.	10.2	>11.6	56.1	•••	•••	•••	1.50	•••	•••	•••
bcc			Ba	Eu	Ba	Eu	Ba	Eu	Ba	Eu	Ba	Eu
(110)	12	Gol.	•••	•••	•••	•••	0.30	0.45	0.57	0.63	538	541
(200)	6	Wil.	5.15	6.17	42.6	51.0	•••	•••	1.50	1.50	•••	•••

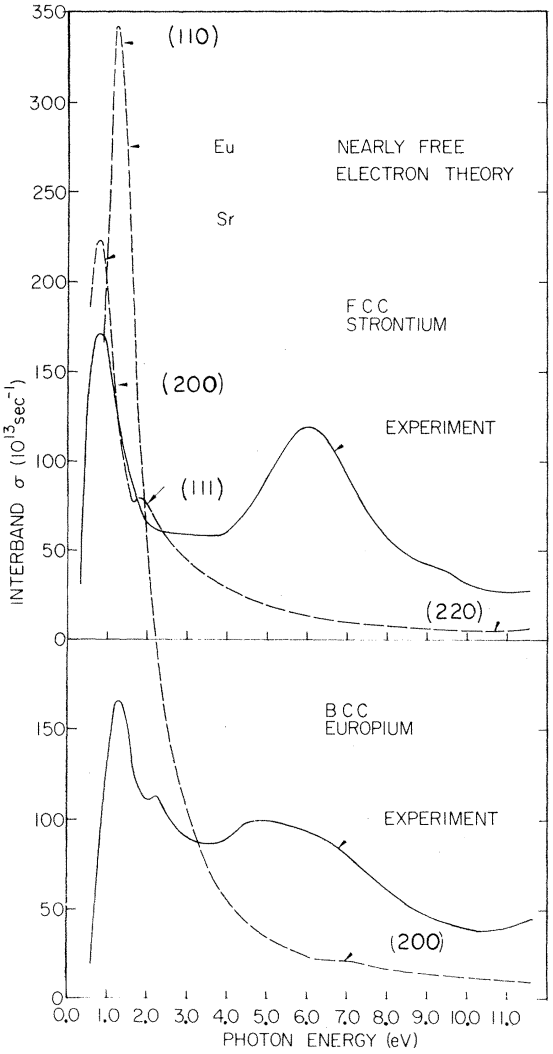

FIG. 28. Comparison of observed interband σ with that predicted in the nearly-free-electron theory for fcc Sr and bcc Eu. Pieces of structure in the theoretical curves are annotated with the Bragg reflection planes from which they arise.

served peaks in the uv.

It should be emphasized that while the nearly-free-electron model experiences some slight success in explaining the observed structure in σ in the visible for the two bcc metals, the fact that there is no combination of single Bragg plane reflections and/or arbitrary but reasonable pseudopotential Fourier components which can account for the structure in σ occurring in the uv for any of these metals suggests that any explanation of the electronic structure of these materials and particularly the prominent structure observed in the uv must go beyond the simple assumptions of the nearly-free-electron model.

2. *Band Calculations and d Hybridization*

The inability of the nearly-free-electron model to describe the optical constants of these metals, particularly at uv frequencies, implies an electronic coupling to the lattice which goes well beyond the assumption of a single Bragg plane interaction. Spectroscopic data showing empty d states lying a mere 1.15 eV above the s valence states of atomic Ba and 2.25 eV above the s valence states of atomic Sr[41] would seem to indicate that the breakdown of the nearly-free-electron theory arises from strong d-band mixing. This interaction has been confirmed by recent band-structure calculations.

The earliest band-structure calculations on any of these metals was carried out on the alkaline-earth metals by Vasvari *et al.*[10] using the model potential method. This study confirmed the existence of strong d-band mixing near the Fermi level in both Ba and Sr. Recently, Johansen[9] has performed a relativistic augmented-plane-wave (RAPW) band calculation on Ba confirming the d mixing near the Fermi level, but unfortunately the resultant band structure is obscured by the presence of the empty $4f$ bands just above E_F. The $4f$ levels are quite sensitive to exchange, and thus their positions shown in this calculation are quite uncertain.

What is probably the most useful band calculation for the purpose of explaining the observed optical constants of the bcc metals was carried out by Freeman, Dimmock, and Furdyna[8] on bcc Eu using the APW method. This is the only band calculation on any of these four metals which was carried to high enough frequency to allow comparison with the uv structure in our observed optical constants, and does not suffer from the distortion related to $4f$-band mixing common to other band calculations. The results of this Eu band calculation are shown in Fig. 29.

It was first suggested by Anderson and Loucks[42] that band-structure calculations on Ba and Eu would show quite similar electronic structures. This has since been confirmed by Johansen.[9] Because these similarities in the electronic structures of bcc Ba and Eu as well as fcc Sr and Yb have also been shown to exist in the experimental observations of these metals, attempts to correlate band calculations to the optical constants reported in this paper will be restricted to a single bcc metal Eu and a single fcc metal Sr, consistent with the comparison to the nearly-free-electron theory shown in Fig. 28.

One of the difficulties inherent in describing the electronic properties of a material in terms of its band structure is that band calculations are normally available only along symmetry lines of the

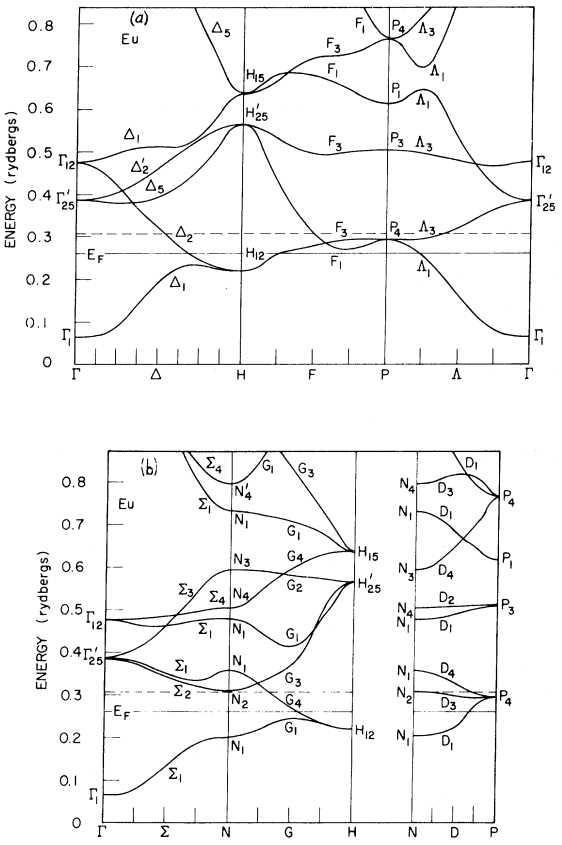

FIG. 29. APW band calculation for bcc Eu by Freeman, Dimmock, and Furdyna (Ref. 8).

Brillouin-zone volume. Such plots do not yield any direct information on effects of interband transitions within the zone volume. In Fig. 30 the energy differences between filled and empty bands of bcc Eu, and filled and empty energy bands of fcc Sr have been plotted along symmetry lines. In order to better estimate the volume effects which occur within the Brillouin zone, each symmetry point in the band structure has been marked by "*P*" if it is a corner of the Brillouin zone or "*F*" if it is a face of the zone. The number of physically equivalent points within the zone is also shown.

The band calculation on Eu by Freeman *et al.* and a band calculation on the fcc phase of Ba by Vasvari *et al.* [10] normalized to the electronic density of Sr were used for the plots of Fig. 30. There are, unfortunately, no reliable direct band calculations on either fcc metal which extend over as large an energy range as the normalized Ba calculation which was used. None of the fcc calculations included density-of-states calculations so that the Fermi level used in determining the filled and empty bands of Sr for Fig. 30 had to be determined from the free-electron Fermi level. Freeman *et al.* [8] calculated the density of states from their band calculation so that E_F, for Eu could be more accurately determined. The energy differences shown between filled and empty bands in the band calculation of Eu were first plotted by Müller, [7] and are plotted for only those transitions which are not forbidden by symmetry. The energy differences for the Sr band structure are plotted between all filled and empty bands with no regard to symmetry.

A qualitative comparison of the plots of ΔE for Eu and Sr on Fig. 30 may be made with the plots of the experimental and nearly-free-electron interband optical conductivities of these two metals shown in Fig. 28. We immediately note that the onset of strong interband transitions predicted by the band calculations occurs at a lower frequency for the fcc Sr than for the bcc Eu. This is in agreement with experimental observations. One also notes that while the Eu band structure implies that a strong onset of interband transitions should occur between 1.5 and 2.0 eV near the N symmetry point, the possibility of strong transition along all symmetry lines and points occurs in the energy range from 3.5 to 5.5 eV. No such higher-energy transitions are apparent in the fcc calculations on Sr. One reason may be that the calculation was not carried to high enough energy. A summary of the results of comparing Figs. 28 and 30 is given in Table IV. The energies of dominant pieces of observed structure in the optical conductivity are listed under "experimental σ," while the energies

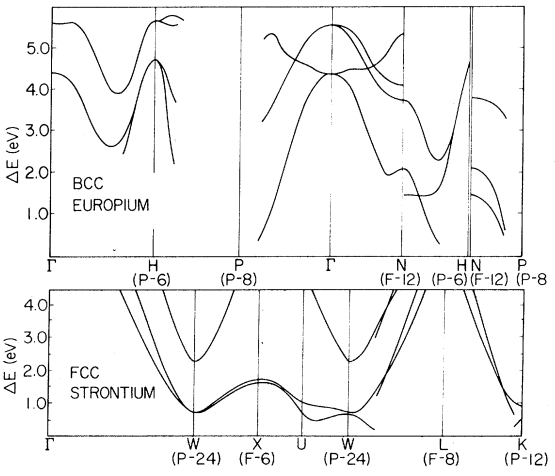

FIG. 30. Energy differences between filled and empty bands plotted along symmetry lines in the Brillouin zone for bcc Eu and fcc Sr. The number of equivalent points or faces in the zone are annotated in parentheses by "*P*" or "*F*," respectively.

TABLE IV. Comparisons of experimentally determined peak positions in the optical conductivity of Eu and Sr from the present study and work of Müller (Ref. 7) with the "critical-point" energies obtained from band calculations for Eu (Ref. 8) and Sr (Ref. 10).

	Experimental σ				Band calculations	
	Present results		Müller			
	Visible	uv	Visible	uv	Visible	uv
Sr	0.8	6.0	•••	•••	(W) (X) 0.7 – 1.7 (W) 2.3	•••
Eu	1.3		1.1	•••	(N) 1.4	(N) (Γ) (H) 3.6, 4.3, 4.6
	2.2	4.7	2.4		(N) 2.1	(N) (Γ) (H) 5.2, 5.4, 5.5

of possible transitions at various symmetry points are given under "band calculations." Transitions may be forbidden right at certain of the symmetry points listed, but are included anyway to account for transitions near these points. The comparison made in Table IV is of the same form as a comparison previously made by Müller on Eu.[7] We have thus included in Table IV the peak positions of the dominant pieces of structure in σ which were observed by Müller in Eu. It should be mentioned, in this regard, that the peak positions obtained for Eu in the visible region by Müller are not in exact agreement with those reported in the present study, although they are within 0.2 eV of the present result. Comparable agreement was also observed in the results obtained on Ba and Yb in these two studies.

The above rather simple comparison of bcc Eu and fcc Sr band structures with the experimental optical conductivity seems to indicate that while both band calculations are successful in qualitatively interpreting the structure which occurs near the onset of interband transitions, only the bcc calculation on Eu shows any sign of the possible occurrence of structure at higher energies. As has been mentioned, any comparison of experimental data with band structure plotted along symmetry lines is obscured by the inability of accounting for volume effects in the Brillouin zone. A more quantitative comparison of band calculation and optical constants may be obtained for bcc Eu by utilizing the density-of-states calculation carried out by Freeman *et al.* on this material. It is well known in what is sometimes called the nondirect-transition model [43] that if optical matrix elements between all filled states and all empty states of a material can be assumed constant, then $\omega\sigma$ for that material is proportional to the convolution of the filled and empty density of states. Although the constant-matrix-element assumption ignores the $\vec{k}$-conservation optical selection rule, this assumption may not be that bad in a material such as Eu which has strong d-band mixing.[44,45]

In Fig. 31, the convolution of the filled and empty densities of states available from the band calculation of Freeman *et al.* is plotted versus optical excitation energy and compared with an experimental plot of $\omega\sigma$ for Eu. Also included is a theoretical plot of $\omega\sigma$ resulting from the nearly-free-electron model.

If one can assume that the constant-matrix-element assumption is not totally unreasonable, then one can make some rather important observations from the plot of Fig. 31. The convolved density of states from Freeman, Dimmock, and Furdyna is of an arbitrary scale so that quantitative comparisons with the experimental $\omega\sigma$ should not be made. Nevertheless, the positions of the two large pieces of structure in this convolved density of states qualitatively confirms the experimentally observed presence of a strong onset of interband transitions near 1 eV followed by a second broad piece of structure in the uv.

It is most important to note that the presence of structure in the uv which was suggested by the simple band energy difference plots in Fig. 30 is confirmed in this analysis which includes volume effects in the Brillouin zone. Of possibly greater

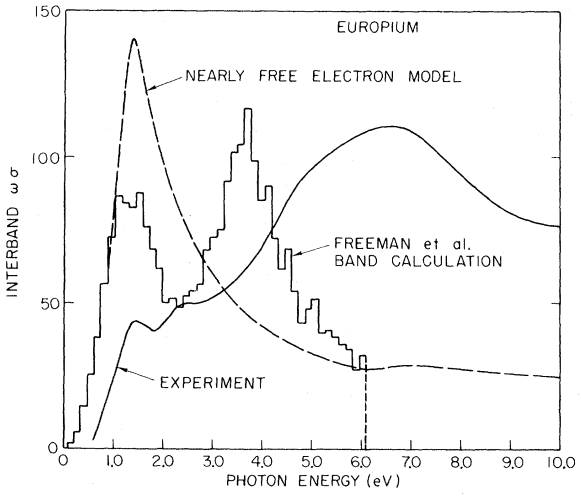

FIG. 31. Comparison of Eu $\omega\sigma$ as determined from the results of the present experimental study, with $\omega\sigma$ as calculated in the nearly-free-electron theory, and $\omega\sigma$ as approximated by ignoring matrix-element effects and convolving the filled and empty densities of states calculated in Freeman, Dimmock, and Furdynas's Eu band calculation (Ref. 8).

significance, however, is the fact that this uv structure in the convolved density of states peaks at a noticeably lower energy than does the uv peak in the experimental $\omega\sigma$. Even the structure in the visible region associated with the onset of interband transitions is somewhat shifted to lower energies in the convolved density of states than is actually observed in the experimental $\omega\sigma$. This may suggest a systematic contraction of the energy scale associated with Freeman, Dimmock, and Furdyna's band calculation.

In comparing the success of these most recent band calculations with the ability of the nearly-free-electron model to explain experimentally observed structure in the optical conductivity, one first has to conclude that only a breakdown of the nearly-free-electron theory, such as occurs in these band calculations, can explain the small magnitude of the peak in the lowest-lying structure in the optical conductivities of the two bcc metals (see both Figs. 25 and 28). It has been shown that the nearly-free-electron model is moderately successful in explaining the onset of interband transitions in the two fcc materials. In no way, however, can the nearly-free-electron model explain the strong piece of structure present in the uv region of the experimental optical conductivities of all four of these metals. This high-energy structure, although occurring at slightly lowered energy, is quite prominent in the band calculation on bcc Eu, and would presumably have been present in a band calculation on fcc Sr carried to high enough energy.

V. CONCLUSIONS

The extreme care taken in our reflectance measurements and the generation of optical constants ϵ_1, ϵ_2, α, and σ has been extensively described in the preceding text. Accuracy of the optical constants was estimated at better than ± 20%, and this accuracy was confirmed in the good agreement between loss-function peak positions obtained for the alkaline-earth metals in Kunz's[25] high-energy electron-loss experiments (7.1 eV for Ba; 8.1 eV for Sr) and the peak positions (7.33 eV for Ba; 8.27 eV for Sr) obtained in calculations from the optical constants of the present study.

The physical interpretation and significance of the optical constants obtained for these metals may be conveniently divided into those factors relating to atomic-oscillator strengths and atomic transitions, and those factors relating to transitions between electronic states of the crystal as a whole. These distinctions are sharply drawn in the discussions that follow.

Comparisons of the optical constants of the two fcc metals Sr and Yb, and the two bcc metals Ba and Eu failed to indicate any additional strong structure or additional oscillator strength in the two rare-earth metals which could be unambiguously attributed to transitions from $4f$ electrons. This failure to observe strong evidence of transitions from the $4f$ electrons in Eu and Yb must be viewed in light of recent soft x-ray photoemission (ESCA) measurements by Brodén, Hagström, Hedén, and Norris[28] indicating that the $4f$ electrons lie between 2.0 and 3.0 eV below the Fermi level in both of these metals. The only anomalous structure observed in the rare-earth metals was the weak piece of structure observable between 2.5 and 3.0 eV in both reflectance and optical constants of fcc Yb, but not observed at corresponding energies in the alkaline-earth fcc Sr. While we observed no evidence for strong transitions from $4f$ electrons, the energy of this weak structure occurs quite near the energy for the onset of transitions from the $4f$ shell to the Fermi level, and such transitions should be considered as a possible explanation of this structure.

We have suggested that our inability to observe strong transitions from these $4f$ states may be explained in terms of atomic-oscillator strengths governing optical excitations of atomic states. It has been pointed out in the recent work of Fano and Cooper[29] that the total oscillator strength associated with $4f$ to g symmetry-state transitions in atomic Eu and Yb should be ten times as strong as the oscillator strength associated with $4f$ to d symmetry-state transitions. The $5d$ states are the only final states in Eu and Yb of either "g" or "d" symmetry which are accessible within the spectral range of the present study, and we have estimated that these $4f$- to $5d$-like state transitions should account for less than 5% of the total $4f$ oscillator strength, or < 0.35 electrons/atom in Eu and < 0.7 electrons/atom in Yb. These estimates of weak coupling in $4f$ to $5d$ transitions are also consistent with the weak excitations of $4f$ electrons observed in recent photoemission studies of the Eu chalcogenides.[34,35] The prediction that the oscillator strength for such transitions in Yb should approach 0.7 electrons/atom and thus be marginally observable against the $6s^2$-like background oscillator strength in Yb lends credibility to our interpretation of the weak structure in Yb optical constants near 3.0 eV as resulting from $4f$ transitions.

The structure which did appear in our comparisons of the interband optical conductivities of the two fcc metals and two bcc metals was found to be extremely well correlated to crystal structure, indicating that the electronic states whose excitations could be observed were strongly influenced by the long-range order of the crystal. The interband σ

curves for the two fcc metals bore only slight dissimilarities. Structure was compared with predictions of the nearly-free-electron theory as well as with predictions of recent band calculations which include strong d-electron effects. The results of these comparisons indicated that the structure obtained in the present study, particularly the strong structure in the uv, was much better correlated with the band-calculation predictions of strong d-electron effects than to the simple predictions of the nearly-free-electron theory. We believe that the strong pieces of structure observed in the uv in the present study provide the best experimental evidence to date for the existence of strong d-electron effects in all four of these metals. Such structure associated with transitions to d-like electrons is sharpest in Sr, and an understanding of these d-electron effects should be facilitated by a better determination of the energy levels of the final d-like states involved in these transitions. Such determinations should be obtainable from the results of photoemission studies presently being undertaken on the alkaline-earth metals Ba and Sr.

ACKNOWLEDGMENTS

The authors would like to thank D. Mosher and P. McKernan of the SEL tube lab for their valuable help in constructing the apparatus used in this experiment. The authors would also like to extend particular thanks to Professor A. Freeman for offering the encouragement to initiate this study and for supplying us with needed Eu band calculations necessary in interpreting the results.

---

†Work supported by the Advanced Research Project Agency through the Center for Materials Research at Stanford University, Calif. 94305

*Work based in part on J. Endriz, Ph. D. thesis, Stanford University, 1970 (unpublished).

[1]F. H. Spedding, J. J. Hanak, and A. H. Daane, Trans. AIME 212, 379 (1958).

[2]J. O. Dimmock, A. J. Freeman, and R. E. Watson, *Optical Properties and Electronic Structure of Metals and Alloys*, edited by F. Abelés (North-Holland, Amsterdam, 1966), p. 237.

[3]F. Herman and S. Skillman, *Atomic Structure Calculations* (Prentice-Hall, Englewood Cliffs, N. J., 1963).

[4]R. J. Maurer, Phys. Rev. 57, 653 (1940).

[5]E. I. Fisher, I. Fujita, and G. L. Weissler, J. Opt. Soc. Am. 56, 1560 (1966).

[6]W. E. Müller, Phys. Letters 17, 82 (1965).

[7]W. E. Müller, Phys. Kondensierten Materie 6, 243 (1967).

[8]A. J. Freeman, J. O. Dimmock, and A. M. Furdyna, Phys. Rev. (to be published).

[9]G. Johansen, Solid State Commun. 7, 731 (1969).

[10]B. Vasvari, A. O. E. Animalu, and V. Heine, Phys. Rev. 154, 535 (1967).

[11]H. E. Bennett and W. F. Koehler, J. Opt. Soc. Am. 50, 1 (1960).

[12]J. Endriz, Ph. D. dissertation, Stanford University, 1970 (unpublished).

[13]C. Schüler, Z. Angew Physik 15, 218 (1963).

[14]Film thickness was measured using a quartz-crystal oscillator, and opacity thickness determined by increasing film thickness until the reflectance values stabilized.

[15]H. E. Bennett and J. O. Porteus, J. Opt. Soc. Am. 51, 123 (1961).

[16]R. H. Ritchie and R. E. Wilems, Phys. Rev. 178, 372 (1969).

[17]J. L. Stanford, H. E. Bennett, J. M. Bennett, E. J. Ashley, and E. T. Arakawa, Bull. Am. Phys. Soc. 13, 989 (1968).

[18]B. P. Feuerbacher and W. Steinman, Opt. Commun. 1, 81 (1969).

[19]J. Endriz and W. E. Spicer, Phys. Rev. Letters 24, 64 (1970).

[20]The general relations follow from the theory of Hilbert transforms.

[21]M. H. Cohen, Phil. Mag. 3, 762 (1958).

[22]Cohen's prediction (Ref. 21) has come under some question in a recent article by N. V. Smith, Phys. Rev. 183, 634 (1969).

[23]K. A. Gschneider, Solid State Phys. 16, 275 (1964).

[24]M. A. Curry, S. Legvold, and F. H. Spedding, Phys. Rev. 117, 953 (1960).

[25]C. Kunz, Ph. D. dissertation, Hamburg, 1966 (unpublished).

[26]E. T. Arakawa, R. N. Hamm, W. F. Hanson, and T. M. Jelinek, *Optical Properties and Electronic Structure of Metals and Alloys*, edited by F. Abelés (North-Holland, Amsterdam, 1966), p. 374.

[27]R. H. Ritchie, Phys. Rev. 106, 874 (1957).

[28]G. Brodén, S. B. Hagström, P. O. Hedén, and C. Norris (unpublished).

[29]U. Fano and J. W. Cooper, Rev. Mod. Phys. 40, 441 (1968).

[30]This is one of the general results obtained for hydrogenic calculations of oscillator strength and is discussed in Ref. 29. See also M. N. Lewis, Natl. Bur. Std. (U.S.) Report No. 2457, 1953 (unpublished).

[31]The unusually high oscillator strength associated with n, $s \rightarrow n$, p transitions is part of a general breakdown of the assumption of a hydrogenic oscillator-strength spectrum which occurs for all allowed transitions of the form $n, l \rightarrow n$, $l+1$. See Sec. 4.5 in Ref. 29.

[32]In Sec. 4.6 of Ref. 29 it is noted that $l \rightarrow l-1$ transitions generally do not depart from the hydrogenic spectrum. Thus, the $4f \rightarrow d$ oscillator-strength spectrum should be hydrogeniclike, and the lowest-lying $4f \rightarrow 5d$ transition should account for noticeably less than 50% of the total $4f \rightarrow d$ strength in analogy with the hydrogen spectrum for which the lowest-lying $1s \rightarrow 2p$ transition accounts for substantially less than half of the total $1s \rightarrow p$ strength.

[33]S. J. Cho (unpublished).

[34]G. Busch, P. Cotti, and P. Munz, Solid State Commun. 7, 795 (1969).
[35]D. E. Eastman, F. Holzberg, and S. Methfessel, Phys. Rev. Letters 23, 226 (1969).
[36]S. T. Manson and J. W. Cooper, Phys. Rev. 165, 126 (1968).
[37]P. Jaegle and G. Missoni, Compt. Rend. 71, 262 (1966).
[38]A. H. Wilson, *The Theory of Metals* (Cambridge U. P., New York, 1936), p. 133.
[39]A. I. Golovashkin, A. I. Kopeliovich, and G. P. Motulevich, Zh. Eksperim. i Teor. Fiz. 53, 2053 (1967) [Soviet Phys. JETP 26, 1161 (1968)]; W. A. Harrison, Phys. Rev. 147, 467 (1966).
[40]A. O. E. Animalu and V. Heine, *Pseudopotentials in the Theory of Metals*, edited by W. A. Harrison (Benjamin, New York, 1966), p. 309.
[41]C. Moore, *Atomic Energy Levels*, Natl. Bur. Std. (U. S.) Circ. No. 467 (U. S. GPO, Washington, D. C., 1949), Vols. 2 and 3.
[42]O. K. Andersen and T. L. Loucks, Phys. Rev. 167, 551 (1968).
[43]C. N. Berglund and W. E. Spicer, Phys. Rev. 136, A1030 (1964); 136, A 1044 (1964).
[44]N. V. Smith, in Proceedings of the Density of States Conference, Natl. Bur. Std., Washington, D. C., 1969 (unpublished).
[45]W. E. Spicer, Ref. 44.

PHYSICAL REVIEW B VOLUME 2, NUMBER 6 15 SEPTEMBER 1970

Size Effects and Doppler-Shifted Cyclotron Resonance of Helicons in Copper†*

L. T. Wood‡† and J. D. Gavenda
Department of Physics, University of Texas, Austin, Texas 78712
(Received 9 January 1970)

Gantmakher-Kaner (GK) oscillations and Doppler-shifted cyclotron resonance (DSCR) of helicons have been investigated in very pure copper with the magnetic field $\vec{B}_0$ and the propagation vector $\vec{q}$ along the [101], [001], and [111] directions. The results are compared with a model Fermi surface proposed by Halse. For $\vec{B}_0 \parallel [101]$, the GK mode is excited by a heavily damped helicon which enhances the effective skin depth for certain values of q. Using a period of 314 ± 7 G for the GK oscillations, we assign a value of $|m_c \bar{v}_z|_{\text{ext}} = (0.648 \pm 0.014) \times 10^{-19}$ g cm sec^{-1} to electrons with orbits near the plane $a|k_z| = 2.675$, where a is the lattice constant, m_c the cyclotron effective mass, and $\bar{v}_z$ the drift velocity along $\vec{B}_0$. The value of $|m_c \bar{v}_z|_{\text{ext}}$ calculated from the model Fermi surface is 0.609×10^{-19} g cm sec^{-1}. Damping of the helicon by open-orbit electrons near the planes $a|k_z| = 4.225$–4.625 has also been observed. For $\vec{B}_0 \parallel [001]$, no GK oscillations were observed; we attribute this to the large-amplitude oscillations in v_z for electron orbits near the plane $a|k_z| = 1.95$. The helicon edge does not appear to be a measure of $|m_c \bar{v}_z|_{\text{max}}$ since $|m_c \bar{v}_z|$ may go to infinity around the necks. For $\vec{B}_0 \parallel [111]$, GK oscillations with a period of 590 ± 7G were observed. This period yields $|m_c \bar{v}_z|_{\text{ext}} = (1.26 \pm 0.02) \times 10^{-19}$ g cm sec^{-1} for electron orbits near the plane $a|k_z| = 3.625$, while the value calculated from the model Fermi surface is 1.34×10^{-19} g cm sec^{-1}. We emphasize that alignment of $\vec{B}_0$ along a crystal axis can be extremely critical, particularly when open-orbit electrons are present.

I. INTRODUCTION

It is well known that electromagnetic waves are generally strongly damped in metals. If, however, one applies a sufficiently strong magnetic field to a pure metal at low temperatures, circularly polarized electromagnetic waves known as helicons can propagate through the metal. The criterion for such waves to propagate is $\omega_c \tau \gg 1$, where ω_c and τ are the conduction-electron cyclotron frequency and relaxation time, respectively. Physically, this means that the electrons are able to complete many cyclotron orbits before they undergo scattering.

Helicons were predicted in 1960 by Aigrain[1] and by Konstantinov and Perel[2] and observed in 1961 by Bowers, Legendy, and Rose.[3] The early helicon experiments[3–7] were directed at determining the Hall coefficients of metals. A proposal by Stern,[8] however, brought to light the fact that helicons could be used to obtain information about the Fermi surface. Stern proposed that helicons could undergo Doppler-shifted cyclotron resonance (DSCR) in much the same way that circularly polarized sound waves undergo DSCR.[9] Suppose a helicon of angular frequency ω and wave number q is propagating in a metal. Let the propagation vector $\vec{q}$ and the applied magnetic field $\vec{B}_0$ both lie along the z axis. An electron with an average velocity $\bar{v}_z$ in the direction of the applied field experiences a Doppler-shifted frequency ω_e given by

$$\omega_e = \omega + q\bar{v}_z \ . \tag{1}$$